

## Article

# Design, Modelling, and Thermodynamic Analysis of a Novel Marine Power System Based on Methanol Solid Oxide Fuel Cells, Integrated Proton Exchange Membrane Fuel Cells, and Combined Heat and Power Production

Phan Anh Duong <sup>1</sup>, Borim Ryu <sup>1</sup>, Jinwon Jung <sup>2,\*</sup> and Hokeun Kang <sup>3,\*</sup><sup>1</sup> Department of Marine System Engineering, Korea Maritime and Ocean University, Busan 49112, Korea<sup>2</sup> Gas Technology Team, Busan Mieum Headquarters, Korea Marine Equipment Research Institute, Busan 49111, Korea<sup>3</sup> Division of Coast Guard Studies, Korea Maritime and Ocean University, Busan 49112, Korea

\* Correspondence: jungjw@komeri.re.kr (J.J.); hkkang@kmou.ac.kr (H.K.)

**Abstract:** A novel maritime power system that uses methanol solid oxide fuel cells (SOFCs) to power marine vessels in an eco-friendly manner is proposed. The SOFCs, gas turbine (GT), steam Rankine cycle (SRC), proton exchange membrane fuel cells (PEMFCs), and organic Rankine cycle (ORC) were integrated together to generate useful energy and harvest wasted heat. The system supplies the exhaust heat from the SOFCs to the methanol dissociation unit for hydrogen production, whereas the heat exchangers and SRC recover the remaining waste heat to produce useful electricity. Mathematical models were established, and the thermodynamic efficiencies of the system were evaluated. The first and second laws of thermodynamics were used to construct the dynamic behavior of the system. Furthermore, the exergy destruction of all the subsystems was estimated. The thermodynamic performances of the main subsystem and entire system were evaluated to be 77.75% and 44.71% for the energy and exergy efficiencies, respectively. With a hydrogen distribution ratio of  $\beta = 0.12$ , the PEMFCs can generate 432.893 kW for the propulsion plant of the target vessel. This is also important for the rapid adaptation of the vessel's needs for power generation, especially during start-up and maneuvering. A comprehensive parametric analysis was performed to examine the influence of changing current densities in the SOFCs, as well as the influence of the hydrogen distribution ratio and hydrogen storage ratio on the operational performance of the proposed systems. Increasing the hydrogen storage ratio ( $\varphi = 0-0.5$ ) reduces the PEMFCs power output, but the energy efficiency and exergy efficiency of the PEMFC-ORC subsystem increased by 2.29% and 1.39%, respectively.

**Keywords:** methanol; SOFC; PEMFC; combined heat and power; Rankine cycle system

**Citation:** Duong, P.A.; Ryu, B.; Jung, J.; Kang, H. Design, Modelling, and Thermodynamic Analysis of a Novel Marine Power System Based on Methanol Solid Oxide Fuel Cells, Integrated Proton Exchange Membrane Fuel Cells, and Combined Heat and Power Production. *Sustainability* **2022**, *14*, 12496. <https://doi.org/10.3390/su141912496>

Academic Editors: Doug Arent, Adam Warren and Xiaolei Yang

Received: 27 August 2022

Accepted: 27 September 2022

Published: 30 September 2022

**Publisher's Note:** MDPI stays neutral with regard to jurisdictional claims in published maps and institutional affiliations.



**Copyright:** © 2022 by the authors. Licensee MDPI, Basel, Switzerland. This article is an open access article distributed under the terms and conditions of the Creative Commons Attribution (CC BY) license (<https://creativecommons.org/licenses/by/4.0/>).

## 1. Introduction

Maritime transport is the most energy-efficient method of shipping goods, accounting for 80% by volume and over 70% by value of international trade [1,2]. Without intervention, the commercial marine shipping industry is likely to increase its emissions, which significantly contribute to global air pollution [3]. To overcome this challenge, the International Maritime Organization (IMO) has initiated numerous guidelines and standards to limit greenhouse gas emissions (GHGs) and manage airborne pollutants. MARPOL Annex VI reduced the maximum permissible content of sulfur for marine fuel from 3.5% to 0.5%, effective from 1 January 2020 [4,5]. The IMO Initial Strategy aimed to cut down carbon dioxide (CO<sub>2</sub>) emission from maritime transportation by at least 40% by 2030 and the overall annually GHG emissions by at least 50% by 2050 compared to 2008 [6,7]. The guidelines and goals have encouraged the use of innovative technology, sustainable fuel sources, and alternative fuels with permissible carbon emissions for global maritime commerce. Due to its high heating value and renewability, hydrogen has performed as a flexible and

environmentally friendly substitute for meeting rising energy demands. Hydrogen can be used extensively in internal combustion engines (ICE), fuel cells, and gas turbines to generate electricity [8]. Hydrogen as a fuel eliminates harmful emissions, including unburned hydrocarbons, aromatic compounds, soot, sulfur oxides, and smoke [9]. However, due to its high volumetric density, its storage and transportation requirements must be carefully considered, especially when hydrogen is used for marine vessels, which requires a large storage volume and a shorter distance for transport [10]. This is the biggest disadvantage of the use of hydrogen in vessels, and there is a need for alternative fuel as a hydrogen carrier. Recently, developments have demonstrated that methanol, as a hydrogen source with high hydrogen content, is a potential and promising ship fuel for reducing SO<sub>x</sub> and CO<sub>2</sub> emissions, resulting in minimal climate change and green shipping targets [11].

Methanol (CH<sub>3</sub>OH) is a colorless, clear liquid that is flammable, volatile, and has an alcoholic smell. Methanol is known for its toxicity and as a polar organic solvent. However, according to a study by Adamson et al. [12], methanol is still recommended for its high level of safety when compared to other hydrogen carriers and fuels. Methanol is easy to handle in its liquid form and has the following properties: a boiling point of 64.7 °C, high energy density, a high octane rating [13], and is environmentally beneficial [14]. In addition, at normal conditions, methanol is simple to store and recharge and safe to handle [15,16]. Therefore, methanol is a viable fuel candidate for internal combustion engines and other maritime applications, such as fuel cells [17]. Renewable liquid methanol is a potential fuel for fuel cells due to its high volumetric energy density and low cost.

There are several kinds of fuel cells, and each individual kind has its own fuel, cost, application, and efficiency characteristics. Due to having benefits over ICEs, including high efficiency, reduced noise, less air pollution emissions, and greater efficiencies, researchers and manufacturers are currently investigating methanol connected to fuel cells. Depending on the type and operating temperature of the fuel cells, a reformer can either supply methanol to the fuel cells directly or indirectly. The two most common kinds of fuel cells, which could be fitted with methanol systems, are SOFCs and PEMFCs. There are only a few experimental reports for other forms of fuel cells, including those with alkaline and alkaline membranes, that are currently being developed [7]. Due to its molecular characteristics, methanol can be reformed at a lower temperature (around 250 °C) than other fuel sources [18]. PEMFCs require pure hydrogen [19–23] (indirectly using methanol by reforming), whereas SOFCs can use methanol directly [24,25]. Because methanol has great potential to be combined with SOFCs and PEMFCs, there are numerous studies on methanol as a fuel and its application in marine fuel cells.

Laosiripojana et al. [26] experimented with the methanol-reforming process in a SOFC system with a CeO<sub>2</sub> surface area. They demonstrated that 100% methanol will be decomposed at an operating temperature of 850 °C, with no evidence of carbon on the surface area. Methanol is strongly recommended as a hydrogen alternative fuel for SOFC, and CeO<sub>2</sub> (HAS) is the preferred catalyst for direct methanol SOFCs. Haseltalab et al. [27] conducted an initial study on the energy management issue of SOFC-based propulsion systems for marine vessels. They presented that, compared to classical diesel-electric propulsion, the suggested integrated SOFC system can reduce CO<sub>2</sub> emissions by 53% and increase fuel utilization efficiency by 21%. SOFCs demonstrate great application potential for marine vessels, owing to high energy efficiency, environmental friendliness, and adaptability to a broad range of fuels. Xu et al. [28] proposed and evaluated a methanol SOFC system, constructed a two-dimensional model to simulate the methanol decomposition process, and demonstrated that, at operating conditions of 0.55 V, 1703 K, and the same molar flow of the feed stream and methanol, the peak power density was 10,220 Wm<sup>-2</sup>. The increase in temperature from 898 to 1173 K dramatically improves power output as a result of increased exhaust gas flow rates, increased ion conduction by the electrolyte, and the increased electrochemical reaction kinetics of the electrodes. Zhou et al. [29] optimized the 30 kW SOFC integrated system with methanol as the fuel and concluded that the electrical and thermoelectric efficiencies obtained were 54% and 88.8%, respectively, under

the operating conditions. Methanol as fuel is more practical than methane (CH<sub>4</sub>) due to its improved reforming water recycle (RWR) performance. Zhang et al. [30] investigated Cu–Ce<sub>0.8</sub>La<sub>0.1</sub>Sm<sub>0.1</sub>O<sub>2-δ</sub> and Cu–Ce<sub>0.8</sub>Nd<sub>0.1</sub>Sm<sub>0.1</sub>O<sub>2-δ</sub> as a material for the anode of a methanol SOFC and reported that, at 650 °C,  $2.1 \times 10^{-5} \text{ cm} \cdot \text{s}^{-1}$  of the exchange coefficient of the oxygen surface,  $2.2 \times 10^{-5} \text{ cm}^2 \cdot \text{s}^{-1}$  for the oxygen chemical coefficient was obtained. The increased oxygen activity in the support encourages the use of Cu-based cermet anodes within the IT range. Duong et al. [31] designed SOFCs for a combined system in a ship and showed that the energy efficiency of the integrating system expanded by 10.59% over the SOFCs electrical efficiency. SOFCs are promising for ship propulsion, but their high operating temperature requires a longer start-up and preparation period. Herdem et al. [32] modeled a high-temperature PEMFC (HT-PEMFC) system with methanol as the fuel and discovered that increasing the molar ratio of CO in reformat gas in a low steam-to-carbon ratio gave a high temperature in the reformer. At a higher hydrogen utilization value, the heat generated from the cell stacks significantly decreased. Additionally, at a 0.8 fuel utilization factor, under 180 °C of cell temperature, and a consumption of 5.2 kg of fuel over 20 h, the PEMFCs can generate 350 kW of power. Wang et al. [33] performed an exergy evaluation of a methanol PEMFC system and showed that the heat exchanger and catalytic reformer are the devices that lose the most exergy, with ratios of 25.03% and 24.95%, respectively. The optimal water to methanol and air to methanol ratios were found to be between 1.5–2.0 and 1.5, respectively.

In order to increase the efficiency of the fuel cells in a combined system, it would be ideal for the hydrogen to be extracted from methanol using waste heat from the SOFCs, with the pressure swing adsorption producing pure hydrogen to supply to the PEMFCs. This would mean that methanol SOFCs could be used as the main power supply for the system, and the waste heat from its exhaust gas could be reused as the heat source for methanol-reforming and the purification system, which would provide additional hydrogen for the PEMFCs and the hydrogen storage tank. The combination of SOFCs and PEMFCs in an integrated power generation system has particular significance for maritime vessels that require rapid response during start-up and maneuvering regimes and constant power during seagoing regimes. Owing to the low operating temperature of the PEMFCs, the hydrogen storage and PEMFC system could immediately generate power for the propulsion plant, whereas for SOFCs, which operate at a higher temperature, this would utilized primarily in stable seagoing conditions. This study proposed and evaluated a novel combined system using SOFC-PEMFC-GT and waste heat recovery cycles, which utilize methanol as a marine-specific fuel. The specific targets of this research are listed below.

- To design and analyze the integrated system with multiple generations of various useful outputs;
- To investigate the thermodynamic aspects of the whole suggested system;
- To implement parametric studies to estimate the reaction of the power plant and subsystem under a variety of influencing factors.

The following are the novel aspects of this study.

- The use of methanol as a potential hydrogen carrier for marine applications;
- The innovation and design of a novel integration system called SOFC-GT-SRC-PEMFC-ORC, which is targeted for use in the existing marine vessel;
- The comprehensive analysis of a methanol-reforming and purifying system using thermodynamic laws;
- The designation of an exhaust heat recovery system for improving the system efficiency;
- The application of the novel combined system in marine vessels to solve current matters surrounding fuel cells for vessels.

The remaining seven sections of this study are structured as follows: Section 2 presents the proposed integrated system and provides background information on methanol SOFCs



Figure 2 depicts the design specifics of the designed methanol SOFC-GT-SRC-PEMFC-ORC combined system. The methanol is supplied to the SOFC-PEMFC waste heat recovery integrated system through a fuel gas supply system (FGSS). Before providing methanol to the SOFC and PEMFC, a methanol-reforming system first heats and reforms the methanol. After the electrochemical reaction in the SOFCs, the exhaust gas is completely combusted in the afterburner. The heat generated by those processes boosts the temperature of the exhaust gases. The exhaust gas is subsequently used to generate additional energy in the GT and Rankine cycles. Therefore, waste heat from the SOFCs is utilized and transferred by a series of regenerations. Below is a description of the cycles' essential components and operating principles.

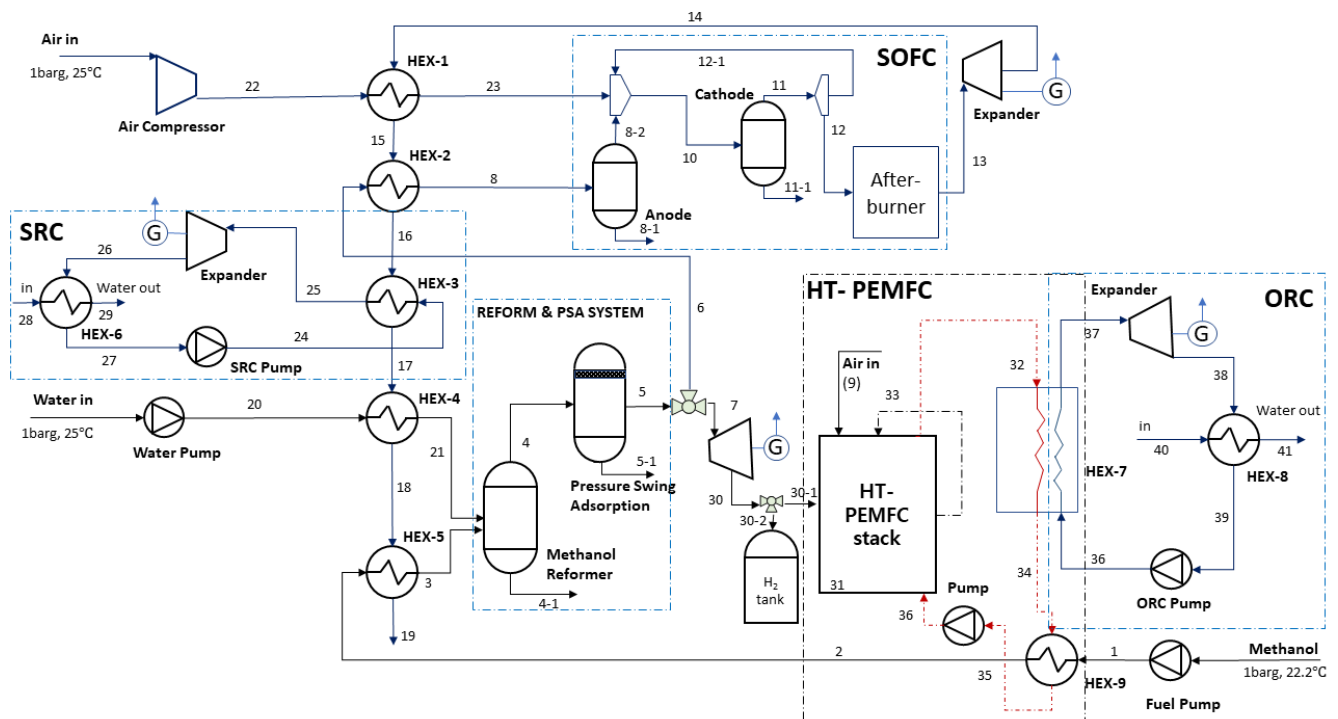


Figure 2. Diagram of the SOFC-GT-SRC-PEMFC-ORC system, using methanol as fuel.

As illustrated in Figure 2, the methanol fuel pump is designed to increase pressure in preparation for the methanol-reforming system. The fuel is then supplied to the heat exchanger, HEX-9, in order to recover the waste heat from the PEMFCs cooling oil and preheat the liquid methanol. An aqueous methanol solution is heated to the superheated temperature in the HEX-5. In parallel, the fresh water from the tank is heated by HEX-4 and pressurized by a water pump before being supplied to the methanol-reformer devices. The vapor mixture enters the reformer, where it undergoes chemical reactions to produce hydrogen. The heat required for the reaction and evaporation is provided by the waste heat from the SOFCs. Following the reformer, the produced gas contains hydrogen as well as incompletely reacted methanol gas, CO, CO<sub>2</sub>, and water vapor. Using pressure swing adsorption (PSA), the pure hydrogen is extracted from the split gas mixture, whereas the residual CO and CO<sub>2</sub> are separated and released. The separated hydrogen is sent to the three-way control valve, which is used to adjust the amount of hydrogen supplied to the SOFCs and PEMFCs. The distribution ratio of hydrogen to the PEMFCs is set to 0.12 in the base case.

SOFC system: first, two heat exchangers use the exhaust heat from the SOFCs to pre-heat the compressed air and hydrogen in series. As a result, the compressed air and hydrogen can obtain the required input temperature for the SOFCs. After preheating, the SOFCs undergo reformation and electrochemical processes. In addition to generating considerable heat, these reactions also produce electricity (by transforming chemical energy

into electrical energy). The DC electricity is then converted into AC before being sent to the electrical power system in the vessel.

**SRC:** The waste heat from the SOFCs can be harvested using heat exchangers, such as HEX-3. The SRC pump initially increases the water pressure in the SRC. The fluid proceeds to the heat exchanger, HEX-3, where its temperature increases. The reversible heat pump is then powered by high-pressurized steam (stream 25), which is depressurized in the expander to generate additional electrical energy. The heat exchanger HEX-6 condenses and transfers the heat to the new cooling water from the saturated water mixture (stream 26). This water, with a temperature of 68.06 °C, will be used to accommodate the sailors onboard the ship.

**The methanol-reforming and hydrogen purifying system:** In the reformer, a methanol–water mixture can be transformed to reformat gas with the participation of catalysts. The two most common catalysts for methanol steam reforming are metal-based and copper-based [34]. In this research, a CuZn base, which is highly active at low temperatures and relatively inexpensive, was considered as the catalyst. After being reformed from methanol, the production gas, which includes CO, CO<sub>2</sub>, hydrogen, and water vapor, is supplied to the PSA, where pure hydrogen is separated from the other produced gases.

**PEMFC system:** The generated pure hydrogen (stream 30-1) is provided to the HT-PEMFC subsystem, whereas the surplus hydrogen (stream 30-2) supplies the hydrogen storage tank. During system startup, the hydrogen tank can be used to supply the system with hydrogen. The pressure regulators between the hydrogen tank and PEMFCs can be altered based on the operational conditions of the fuel cells. Hydrogen is extracted from the reforming and purification system (stream 7) under high pressure and temperature. Thus, the expander is designed to regulate the pressure and temperature of the hydrogen being provided to the HT-PEMFC. The unreacted hydrogen, after PEMFC (stream 33), is also recovered and reused to improve system efficiency. A compressor and heat exchanger heat and pressurize the ambient air to stack the operating temperatures. The heat exchanger receives the generated water and unreacted air, heating the intake gas. The HT-PEMFC stack produces heat and electricity during its operation. The waste heat recovery subsystem of the ORC receives heat transfer oil, which transfers heat from the stack (HEX-7). The organic working fluid is vaporized by absorbing heat from the cooling oil in the evaporator. The superheated stream from the organic working fluid (stream 37) provides the expander and drives it to produce electricity. Before entering the ORC pump, the working fluid is condensed in the condenser, HEX-8. Before entering the cycle, the working fluid is pressurized to the required pressure of the ORC pump.

### 3. Thermodynamic Model

#### 3.1. Equations for Thermodynamic Balance

The equations for thermodynamic balance used in the integrated systems, such as the balance of mass and energy, entropy, and exergy destruction rate, are covered in this section. Using the techniques for examining energetic and exergetic efficiency, comprehensive modeling and analysis of the thermodynamics was conducted. In addition, some considerations for the thermodynamic evaluation are provided. Here are the assumptions underlying the presented model:

- The entire system is anticipated to perform under steady-state circumstances;
- The variations in kinetic and potential energy are negligible;
- It is assumed that no heat is lost to the environment through the pipe connections;
- The pipeline pressure drops are not taken into consideration.

Mass balance equation:

The four equilibrium equations, including mass, energy, entropy, and exergy, under steady-state conditions, are made and discussed. Consider a thermodynamically modeled component to be a control volume (CV). There is no mass change in the CV under a steady-state [35,36]:

$$\sum_{in} \dot{m}_{in} = \sum_{out} \dot{m}_{out} \quad (1)$$

$$\sum_{in} \dot{m}_{in} - \sum_{out} \dot{m}_{out} = \frac{dm_{CV}}{dt} = 0 \quad (2)$$

where  $\dot{m}$  is the mass flow rate. Total mass flow rates into and out of a control volume are subtracted to determine mass variation in CV.

- Equations for energy balance:

Energy conservation is built upon the first law of thermodynamics [37]:

$$\sum_{in} \dot{m}_{in} h_{in} + \dot{Q}_{in} + \dot{W}_{in} = \sum_{out} \dot{m}_{out} h_{out} + \dot{Q}_{out} + \dot{W}_{out} \quad (3)$$

$$\dot{Q} - \dot{W} + \sum_{in} \dot{m}_{in} \left( h_{in} + \frac{V_{in}^2}{2} + gZ_{in} \right) - \sum_{out} \dot{m}_{out} \left( h_{out} + \frac{V_{out}^2}{2} + gZ_{out} \right) = 0 \quad (4)$$

where  $\dot{Q}$ ,  $\dot{W}$ , and  $h$  represent the rate of heat transfer, mechanical power, and specific enthalpy, respectively.

The precise kinetic and potential energy connected to the “enter” and “leave” mass flow rates were ignored and thought to be insignificant in this thermodynamic analysis [35]:

$$\dot{Q}_{in} + \sum_{in} \dot{m}_{in} (h_{in}) = \dot{W}_{out} + \sum_{out} \dot{m}_{out} (h_{out}) \quad (5)$$

- Equations for entropy and exergy balance:

The equations for the entropy and energy balances were assessed using the second law of thermodynamics. In a CV, the rate of entropy change is zero under steady-state circumstances.

$$\sum_{in} \dot{m}_{in} s_{in} + \sum \left( \frac{\dot{Q}}{T} \right) + \dot{S}_{gen} = \sum_{out} \dot{m}_{out} s_{out} \quad (6)$$

$$\sum_k \frac{\dot{Q}_k}{T_k} + \sum_{in} \dot{m}_{in} (s_{in}) + \dot{S}_{gen} - \sum_{out} \dot{m}_{out} (s_{out}) = \frac{dS_{CV}}{dt} = 0 \quad (7)$$

or

$$\sum_k \frac{\dot{Q}_k}{T_k} + \sum_{in} \dot{m}_{in} (s_{in}) + \dot{S}_{gen} = \sum_{out} \dot{m}_{out} (s_{out}) \quad (8)$$

where  $s$ ,  $T$ , and  $\dot{S}_{gen}$  represent specific entropy, temperature (°C), and entropy of process, respectively.

In the control volume, the exergy rate of change is zero under steady-state conditions.

$$\sum_k \left( 1 - \frac{T_0}{T_k} \right) \dot{Q}_k - \dot{W}_{out} + \sum_{in} \dot{m}_{in} (ex_{in}) - \sum_{out} \dot{m}_{out} (ex_{out}) - \dot{E}x_{dest} = \frac{dEx_{CV}}{dt} = 0 \quad (9)$$

$$\sum_k \left( 1 - \frac{T_0}{T_k} \right) \dot{Q}_k + \sum_{in} \dot{m}_{in} (ex_{in}) = \sum_{out} \dot{m}_{out} (ex_{out}) + \dot{W}_{out} + \dot{E}x_{dest} \quad (10)$$

- Exergy destruction rate and specific exergy:

The entropy production rate can be used to compute the exergy destruction rate for each CV or component.

$$\dot{E}x_{dest} = T_0 \dot{S}_{gen} \quad (11)$$

Here,  $T_0$ ,  $\dot{E}x_{dest}$ , and  $ex$  denote the ambient temperature (°C), exergy destruction rate, and specific exergy, respectively. The total of the physical, chemical, kinetic, and potential exergy is used to determine the specific exergy values:

$$ex_j = ex_j^{ph} + ex_j^{ch} + ex_j^{ke} + ex_j^{pe} \quad (12)$$

The kinetic and potential exergy in this thermodynamic analysis were found to be insignificant and were therefore disregarded. An ideal gas mixture-specific weighted average method was used to determine the specific enthalpy and entropy of the SOFC exhaust gases.

$$ex_j = ex_j^{ph} + ex_j^{ch} \quad (13)$$

The physical exergy in this equation can be calculated as:

$$ex_j^{ph} = (h_j - h_0) - T_0(s_j - s_0) \quad (14)$$

The chemical exergy will be predicted by:

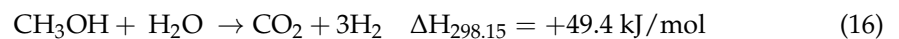
$$ex_j^{ch} = \sum_k x_k (ex_k^{ch} - RT_0 x_k \ln(x_k)) \quad (15)$$

where  $x_k$ ,  $R$ , and  $ex_j^{ch}$  present the mass ratio, gas constant, and specific exergy, respectively.

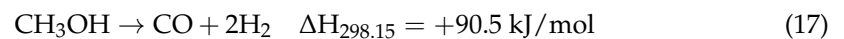
### 3.2. Methanol Steam Reforming

As fuel cells work primarily with hydrogen and oxygen, it is necessary to install a methanol steam-reforming system for methanol PEMFCs. Hydrogen will be produced in this system by heating, reforming, and reacting the aqueous and methanol methods together. The principal chemical reaction can be summed up as follows:

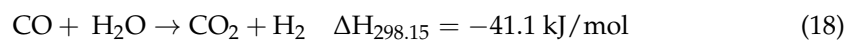
- Endothermic reaction:



- Decomposing reaction of methanol (to produce hydrogen):



- The water-gas-shift reaction (to produce hydrogen):



The catalyst is employed to speed up the reactions and ensure the direction and processing of the reaction as well. In this case,  $\text{CuO}/\text{ZrO}_2$  is selected [38,39].

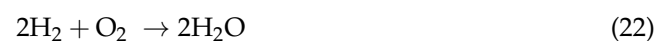
Environmental indices are primarily influenced by CO and  $\text{CO}_2$ . The environmental assessment indicator, which is the system's carbon mass specific emission, is the sum of CO and  $\text{CO}_2$  released during the system's generation in addition to its electric output (MSE) [40,41]:

$$MSE = \frac{3600 (\dot{m}_{\text{CO}} + \dot{m}_{\text{CO}_2})}{W_{\text{net}}} \quad (19)$$

After reforming, hydrogen is provided to the anode of the fuel cells and oxygen to the cathode. The anode and cathode chemical reaction can be summarized:



The overall reaction in the fuel cells is:



In order to obtain thermodynamic equilibrium, the governing process, Gibbs energy, will be minimized in the methanol stream reformer [42–44]:

$$(\Delta G_{system})_{T,P} = 0 \quad (23)$$

In this case, the system's Gibbs energy is equal to the total of chemical species' moles,  $i$ , for the appropriate specific Gibbs energy:

$$G_{system} = \sum n_i \bar{g}_i \quad (24)$$

The activity of a species is the ratio of its fugacity in the system to its fugacity at the standard temperature and pressure (STP) for actual gases:

$$\bar{g}_i = \bar{g}_{fi}^0 + RT \ln \frac{f_i}{f_i^0} \quad (25)$$

Gibbs free energy [45] can be estimated by:

$$G_{system} = \left( \sum n_i [\bar{g}_{fi}^0 + RT \ln(y_i P)] \right)_{gas} + \left( \sum n_i \bar{g}_{fi}^0 \right)_{condensed} \quad (26)$$

$$\min_{n_j} (G_{MSR})_{T,p} = \min_{n_j} \left( \sum_{j=1}^k n_j \bar{G}_j \right) \sum_{j=1}^k n_j \left( G_j^0 + RT \ln \frac{\bar{f}_j}{f_j^0} \right) \quad (27)$$

Due to the conversion of atomic species:

$$\sum_{j=1}^k n_j a_{j,d} = b_d \quad \text{for } 1 \leq d \leq D. \quad (28)$$

The production of hydrogen can be estimated as:

$$y_{H_2} = \frac{\dot{F}_{H_2, out}}{\dot{F}_{Methanol, out}} \times \frac{1}{3} \times 100\% \quad (29)$$

As the reformer and the needed heat for the reforming process are recovered by the exhaust gas from the SOFCs, which is higher than 200 °C, the hydrogen yield of the methanol stream reformat is larger than 95% for the overall process [39].

### 3.3. Model of the SOFC

There are two kinds of SOFC systems: oxygen-ion-conducting electrolytes (SOFC-O) and proton-conducting electrolytes (SOFC-H) [46]. For the SOFC-H, a proton-conducting ceramic electrolyte, such as barium cerate, is preferable, whereas for the SOFC-O, oxygen ion-conducting electrolytes, such as YSZ or SDC, are needed.

Fuel and air utilization ratio

The utilization of methanol can be estimated based on the absolute supply and reaction of the methanol, or the amount of counterpart hydrogen [29]:

$$U_{f-f} = \frac{(Fuel)_{reacted}}{(Fuel)_{provide}} = \frac{(H_2)_{reacted}}{(H_2)_{provide}} \quad (30)$$

The air utilization:

$$U_{f-air} = \frac{(Air)_{reacted}}{(Air)_{provide}} = \frac{(O_2)_{reacted}}{(O_2)_{provide}} \quad (31)$$

The amount of oxygen flow supplied to the cathode can be estimated via the power generated by the SOFCs, ( $P_{SOFC}$ ), divided by the number of transfer electrons, ( $n$ ), and SOFC voltage and Faraday constant 96.458 ( $F$ ), given by:

$$f_{SOFC,O_2} = \frac{P_{SOFC}}{U_{SOFC} \cdot n \cdot F} \left( \frac{\text{mol}}{\text{min}} \right) \quad (32)$$

$$q_{fuel} = \frac{i \cdot N_{Cell} \cdot A_{Cell}}{U_f \cdot n \cdot F} \left( \frac{\text{mol}}{\text{s}} \right) \quad (33)$$

The hydrogen flow provided to the anode is estimated via the main reaction of hydrogen and oxygen in the SOFC:

$$f_{SOFC,H_2} = 2 \cdot f_{SOFC,O_2} \left( \frac{\text{mol}}{\text{min}} \right) \quad (34)$$

The SOFC system's net power output is also computed using the component stack [47–49]:

$$W_{stack} = i \cdot A \cdot V_c \eta_{DA} \quad (35)$$

where  $i$ ,  $\eta_{DA}$ ,  $V_c$ , and  $A$  are the current density ( $\text{A}/\text{m}^2$ ), converter efficiency, actual voltage ( $V$ ), and the surface area ( $\text{m}^2$ ), respectively [48,50].

$$V_c = V_R - V_{loss} \quad (36)$$

where  $V_R$  is cell ideal reversible voltage, therefore:

$$V_{loss} = V_{ohm} + V_{act} + V_{con} \quad (37)$$

In this expression,  $V_{ohm}$ ,  $V_{con}$ , and  $V_{act}$  are the losses of ohmic ( $V$ ), concentration ( $V$ ), and activation ( $V$ ), respectively.

$$V_{ohm} = V_{ohm,a} + V_{ohm,c} + V_{ohm,e} + V_{ohm,int} \quad (38)$$

$$V_{ohm,a} = \frac{i \rho_a (A \cdot \pi \cdot D_m)}{8 \cdot t_a} \quad (39)$$

$$V_{ohm,c} = \frac{i \rho_c (A \cdot \pi \cdot D_m)^2}{8 \cdot t_c} A \cdot (A + 2(1 - A - B)) \quad (40)$$

$$V_{ohm,e} = i \rho_a t_e \quad (41)$$

$$V_{ohm,int} = i \cdot \rho_{int} \cdot \pi \cdot D_m \frac{t_{int}}{w_{int}} \quad (42)$$

$$V_{act} = \frac{2RT}{F \cdot n_e} \text{Arcsinh} \left( \frac{i}{2i_{0,k}} \right) \quad (43)$$

$$V_{con} = \frac{RT}{2F} \ln \left( \frac{1 - \frac{i}{i_{L,H_2}}}{1 + \frac{i}{i_{L,O_2}}} \right) + \frac{RT}{2F} \ln \left( \frac{1}{1 - \frac{i}{i_{L,O_2}}} \right) \quad (44)$$

Moreover, the I–V curve is also employed to define the actual voltage of the SOFC [35,51–55].

Alternatively, the fuel cell's energy efficiency can be computed as:

$$\eta_{en, SOFC} = \frac{\dot{W}_{elect,SOFC}}{\dot{m}_6 h_6 + \dot{m}_{air} h_{air} - \dot{m}_{12} h_{12}} \quad (45)$$

Or [48,56]:

$$\eta_{en,SOFC} = \frac{\dot{W}_{SOFC}}{\dot{m}_6 LHV_{fuel\_6}} \quad (46)$$

where  $\dot{m}_6$  denotes the mass flow rate of hydrogen when entering the SOFC system (kg/h), and  $LHV_{fuel\_6}$  represents the low heating value of hydrogen (KJ/kg).

### 3.4. Model of PEMFC

The PEMFC represents a promising power generation device for maritime application owing to its high power density, low emissions, environmental friendliness, low maintenance, and smooth and silent operation [39]. According to overall working performance, PEMFCs can be divided into two primary types: high-temperature PEMFCs (HT-PEMFCs) and low-temperature PEMFCs (LT-PEMFCs) [57–60]. Compared to LT-PEMFCs, HT-PEMFCs, which typically operate between 120–200 °C, exhibit superior waste heat and CO tolerance [61,62] and are more suitable for energy conversion devices [63]. As water management and pure hydrogen quality are the most important issues for PEMFCs, the current research focuses on HT-PEMFCs own characteristics. The reasons for selecting HT-PEMFCs [32] mainly include: (i) HT-PEMFCs require a lower quality of hydrogen than LT-PEMFCs; approximately 3% CO gas can be tolerated in HT-PEMFCs [64]; (ii) water is in the vapor phase at the high working temperature in HT-PEMFCs, thus, it is not an issue [65]; (iii) compared to LT-PEMFCs, HT-PEMFCs have faster electrochemical kinetics; (iv) HT-PEMFCs are easier and more effective at recovering waste heat [66].

The power generated by PEMFC can be estimated via variable output cell voltage, current density and number of cells:

$$W_{stack, PEMFC} = N_{cell} \cdot V_{cell} \cdot i \cdot A_{cell} \quad (47)$$

$$Q_{stack, PEMFC} = W_{stack, PEMFC} \cdot \frac{(V_{rev} - V_{ave})}{V_{ave}} \quad (48)$$

The supplied hydrogen and air for PEMFCs can be calculated [67] as:

- Mass flow rate of hydrogen:

$$\dot{m}_{H_2, PEMFC} = \lambda_{anode} \cdot M_{H_2} \cdot \frac{N_{cell} \cdot i}{2F} = \lambda_{anode} \cdot M_{H_2} \cdot \frac{N_{cell} \cdot A_{cell} \cdot i}{2F} \quad (49)$$

- Mass flow rate of air:

$$\dot{m}_{air, PEMFC} = \lambda_{cathode} \cdot M_{air} \cdot \frac{N_{cell} \cdot i}{4F \cdot g_{O_2}} = \lambda_{cathode} \cdot M_{air} \cdot \frac{N_{cell} \cdot A_{cell} \cdot i}{4F \cdot g_{O_2}} \quad (50)$$

As for management of heat in PEMFCs, the heat supplied to the evaporator is:

$$Q_{evaporator} = Q_{stack} - Q_{reaction} - Q_{supercritical} \quad (51)$$

The overall efficiency of PEMFCs can be calculated by:

$$\eta_{PEMFC} = \frac{\dot{W}_{PEMFC}}{\dot{m}_{H_2} LHV_{H_2}} \quad (52)$$

Thus,

$$\dot{W}_{PEMFC} = \eta_{PEMFC} \cdot \dot{m}_{H_2} \cdot LHV_{H_2} \quad (53)$$

The actual energy produced can also be used to calculate the electrical efficiency of PEMFCs:

$$\eta_{cell} = \frac{V}{1.25} \quad (54)$$

where 1.25 stands for the maximum open circuit voltage for the vapor-water product, and  $V$  is the actual cell voltage.

### 3.5. Model of Gas Turbine System

After being completely reacted in the afterburner, the exhaust gas supplies the gas turbine, where it expands and produces useful mechanical power. The following equations are employed to calculate the exit temperature:

$$T_{out} = T_{in} (PR)^{(k-1)/k} \quad (55)$$

in which,  $PR = \frac{P_{in}}{P_{out}}$  and  $k = \frac{\sum_i y_i \dot{C}_{p,i}}{\sum_i y_i \dot{C}_{v,i}}$

Isentropic efficiency:

$$\eta_{s,T} = \frac{\sum_i (\dot{n}_i \bar{h}_i)_{in} - \sum_i (\dot{n}_i \bar{h}_i)_{out}}{\sum_i (\dot{n}_i \bar{h}_i)_{in} - \sum_i (\dot{n}_i \bar{h}_i)_{s, out}} \quad (56)$$

Exergy efficiency:

$$\psi_T = \frac{\dot{W}_T}{\sum_i (\dot{n}_i \bar{e}x_i)_{in} - \sum_i (\dot{n}_i \bar{e}x_i)_{out}} \quad (57)$$

The energy and exergy efficiencies of the SOFC-GT subsystem:

- Energy efficiency:

$$\eta_{en,SOFC,GT} = \frac{\dot{W}_{SOFC} + \dot{W}_{GT}}{\dot{m}_6 LHV_{fuel\_6}} \quad (58)$$

- Exergy efficiency:

$$\eta_{ex,SOFC,GT} = \frac{\dot{W}_{SOFC} + \dot{W}_{GT}}{\dot{m}_6 ex_{fuel\_6}} \quad (59)$$

#### Air compressor

The process for determining the gas turbine's isentropic energy and exergy efficiencies is employed for determining air compressor's isentropic efficiency:

$$\eta_{en,Compressor} = \frac{\sum_i (\dot{n}_i \bar{h}_i)_{s,out} - \sum_i (\dot{n}_i \bar{h}_i)_{in}}{\sum_i (\dot{n}_i \bar{h}_i)_{out} - \sum_i (\dot{n}_i \bar{h}_i)_{in}} \quad (60)$$

The air compressor's exergy efficiency:

$$\eta_{ex,Compressor} = \frac{\sum_i (\dot{n}_i \bar{e}x_i)_{in} - \sum_i (\dot{n}_i \bar{e}x_i)_{out}}{\dot{W}_C} \quad (61)$$

#### Electric generator

The excess power of electric generator:

$$\dot{W}_G = \eta_G (\dot{W}_T - \dot{W}_C) \quad (62)$$

#### Heat exchangers

The heat exchanger's hot and cold streams are determined by:

- Hot stream (exhaust gas):

$$\dot{Q} = \sum_i (\dot{n}_i \bar{c}_{p,i})_h (T_{h,in} - T_{h,out}) \quad (63)$$

- Cold stream (fuel or air supply):

$$\dot{Q} = \sum_i (\dot{m}_i \bar{c}_{p,i})_h (T_{c,in} - T_{c,out}) \quad (64)$$

### 3.6. Organic Rankine Cycle

For the control volume and steady state condition, the energy conservation of the ORC is

$$\dot{Q} + \sum \dot{m}_{in} h_{in} = \dot{W} + \sum \dot{m}_{out} h_{out} \quad (65)$$

- ORC input energy:

$$\dot{Q}_{in, ORC} = \dot{m}_{ORC} (h_{32} - h_{34}) \quad (66)$$

- ORC net electric power:

$$\dot{W}_{net, ORC} = \dot{W}_{ORC, Turbine} - \dot{W}_{ORC, Pump} \quad (67)$$

- Energy efficiency of the ORC:

$$\eta_{en, ORC} = \frac{\dot{W}_{net, ORC}}{\dot{Q}_{in, ORC}} \quad (68)$$

- Exergy efficiency of ORC:

$$\eta_{ex, ORC} = \frac{\dot{W}_{net, ORC}}{\dot{E}x_{in, ORC}} \quad (69)$$

### 3.7. Steam Rankine Cycle (SRC)

- The energy balance:

$$\dot{m}_{wf, SRC} h_{16} = \dot{W}_{SRC, T} + \dot{m}_{wf, SRC} h_{17} \quad (70)$$

- The SRC's net power output:

$$\dot{W}_{net, SRC} = \dot{W}_{SRC, Expander} - \dot{W}_{SRC, Pump} \quad (71)$$

Its energy and exergy efficiencies are:

$$\eta_{en, SRC} = \frac{\dot{W}_{net, SRC}}{\dot{m}_{16} (h_{16} - h_{17})} \quad (72)$$

$$\eta_{ex, SRC} = \frac{\dot{W}_{net, SRC}}{\dot{m}_{16} (ex_{16} - ex_{17})} \quad (73)$$

The main components' exergy destruction rates are determined and displayed in Table 2.

**Table 2.** Formulae for the destruction of exergy in the major components.

Components	Exergy Destruction Rate	Equation
SOFC	$\dot{E}x_{22} + \dot{E}x_6 + \dot{E}x_{12-1} - \dot{E}x_{12} - \dot{W}_s = \dot{E}x_{des}$	(74)
Afterburner	$\dot{E}x_{12} - \dot{E}x_{13} = \dot{E}x_{des}$	(75)
Gas Turbine	$\dot{E}x_{13} - \dot{E}x_{14} - \dot{W}_{Gas\ turbine} = \dot{E}x_{des}$	(76)
HEX-1	$\dot{E}x_{22} + \dot{E}x_{14} - \dot{E}x_{23} - \dot{E}x_{15} = \dot{E}x_{des}$	(77)
HEX-2	$\dot{E}x_6 + \dot{E}x_{15} - \dot{E}x_{16} - \dot{E}x_8 = \dot{E}x_{des}$	(78)
HEX-3	$\dot{E}x_{16} + \dot{E}x_{24} - \dot{E}x_{17} - \dot{E}x_{25} = \dot{E}x_{des}$	(79)
SRC turbine	$\dot{E}x_{25} - \dot{E}x_{26} - \dot{W}_{S\_Turbine} = \dot{E}x_{des}$	(80)
PEMFC	$\dot{E}x_{30} + \dot{E}x_{air\ in} - \dot{E}x_{32} - \dot{E}_{out} = \dot{E}x_{des}$	(81)
HEX-7	$\dot{E}x_{32} + \dot{E}x_{36} - \dot{E}x_{34} - \dot{E}x_{37} = \dot{E}x_{des}$	(82)
ORC turbine	$\dot{E}x_{37} - \dot{E}x_{38} - \dot{W}_{O\_Turbine} = \dot{E}x_{des}$	(83)
HEX-4	$\dot{E}x_{17} + \dot{E}x_{20} - \dot{E}x_{18} - \dot{E}x_{21} = \dot{E}x_{des}$	(84)
HEX-5	$\dot{E}x_2 + \dot{E}x_{18} - \dot{E}x_3 - \dot{E}x_{19} = \dot{E}x_{des}$	(85)
HEX-6	$\dot{E}x_{28} + \dot{E}x_{26} - \dot{E}x_{27} - \dot{E}x_{29} = \dot{E}x_{des}$	(86)

The following are the general energy and exergy efficiencies of the whole combined system [35,68,69]:

Energy efficiency:

$$\eta_{en, overall} = \frac{\dot{W}_{elec, overall}}{\dot{m}_{Methanol} LHV_{Methanol}} \quad (87)$$

In these expressions,  $\dot{W}_{elec, overall}$  represents the net power production, subtracting the net power consumption:

$$\begin{aligned} \dot{W}_{elec, overall} = & \dot{W}_{elec, SOFC} + \dot{W}_{Gasturbine} + \dot{W}_{SRC, turbine} + \dot{W}_{independence\ Turbine} \\ & + \dot{W}_{PEMFC} + \dot{W}_{ORC, turbine} - \dot{W}_{Air\ comp} - \dot{W}_{SRC, pump} - \dot{W}_{ORC, pump} \end{aligned} \quad (88)$$

$LHV_{Methanol}$  is the methanol's lower heating value (kJ/kg).

Exergy efficiency:

$$\eta_{ex, overall} = \frac{\dot{W}_{elec, overall}}{\dot{m}_{Methanol} ex_{Methanol}} \quad (89)$$

#### 4. Simulation and Assumptions

The constructed system, SOFC-GT-SRC-PEMFC-ORC, using methanol as a fuel, was simulated utilizing ASPEN-HYSYS V12.1, which provides robust methodologies and a large database for computing physical properties [70,71]. The simulation utilized the Aspen Physical Property System REFPROP function [39,72]. The employed Peng–Robinson (PR) equation of states, the thermodynamic parameters of stream compositions, and the operating conditions were the determining components of the SOFC-PEMFC waste-heat recovery integrated system.

To make the thermodynamic analysis of the system more straightforward, the following assumptions were made:

- ① The methanol assessing the FGSS was 22.2 °C and 101 kPa [73];
- ② The air consisted of 21% O<sub>2</sub>, 79% N<sub>2</sub> at 25 °C, and 101 kPa;
- ③ The heat exchanger's minimum temperature approach was 5 °C.

The boundary conditions of this simulation are demonstrated in Table 3 [35,50].

**Table 3.** System design and operational parameters.

Component	Parameter	Unit	Value
SOFC	Ambient pressure	bar	1.013
	Ambient temperature	°C	25
	Operating Pressure	bar	3.8
	Operating Temperature	°C	878.1
	Quantitatively of cell		15 176
	Current density	A/m <sup>2</sup>	1400
	Active surface area	m <sup>2</sup>	0.25
	Anode thickness	cm	0.0018
	Cathode thickness	cm	0.0018
	Electrolyte thickness	cm	0.0040
	Hydrogen stoichiometric		1.2
	Oxygen stoichiometric		2
	Gas turbine cycle compression ratio		13
	Fuel utilization factor.		85%
PEMFC	Operating pressure	bar	1.2
	Operating temperature	°C	165.8
	Quantitatively of cell		3100
	Active surface area	m <sup>2</sup>	0.06
	Membrane hydration		23
	Membrane thickness	cm	0.016
	Current density	A/m <sup>2</sup>	4300
	Hydrogen stoichiometric		1.2
	Oxygen stoichiometric		2
	Compressor	Isentropic efficiency	%
Pumps	Isentropic efficiency	%	85
Expanders	Isentropic efficiency	%	88
Heat exchangers	Minimum temperature approach	°C	5
Converter	DC-AC converter efficiency	%	98

## 5. Modeling Verification

Table 4 displays the results of the proposed model with methanol as the fuel, which was calculated using our research proposal and results from the literature [48]. The estimated values correspond to results from the literature, and the differential is kept within a reasonable range.

**Table 4.** Resemblance of the simulation results to those from the literature.

Parameter	Modelling	Reported [48]	Different (%)
Temperature of SOFC (°C)	882.7	870	1.37
Gas Turbine inlet temperature (°C)	1140	1201	5.07
Cell voltage (V)	0.73	0.747	2.27
Current Density (A/m <sup>2</sup> )	1400	1429	2.02
SOFC efficiency	52	50.96	1.04

The proposed system can simultaneously generate hot water for the sailors on board the ships and power the propulsion plant and other electrical equipment. It is essential to verify the subsystem because it generates 32.75% of the total generated power.

The operating performance of the PEMFCs and the methanol-reforming and purification subsystems is based on an experiment by Sousa et al. [74] in Figure 3. The results reveal that the model and experimental data are in agreement. One explanation for the minor inaccuracy is that the actual voltage loss (of the fuel cells) was ignored.

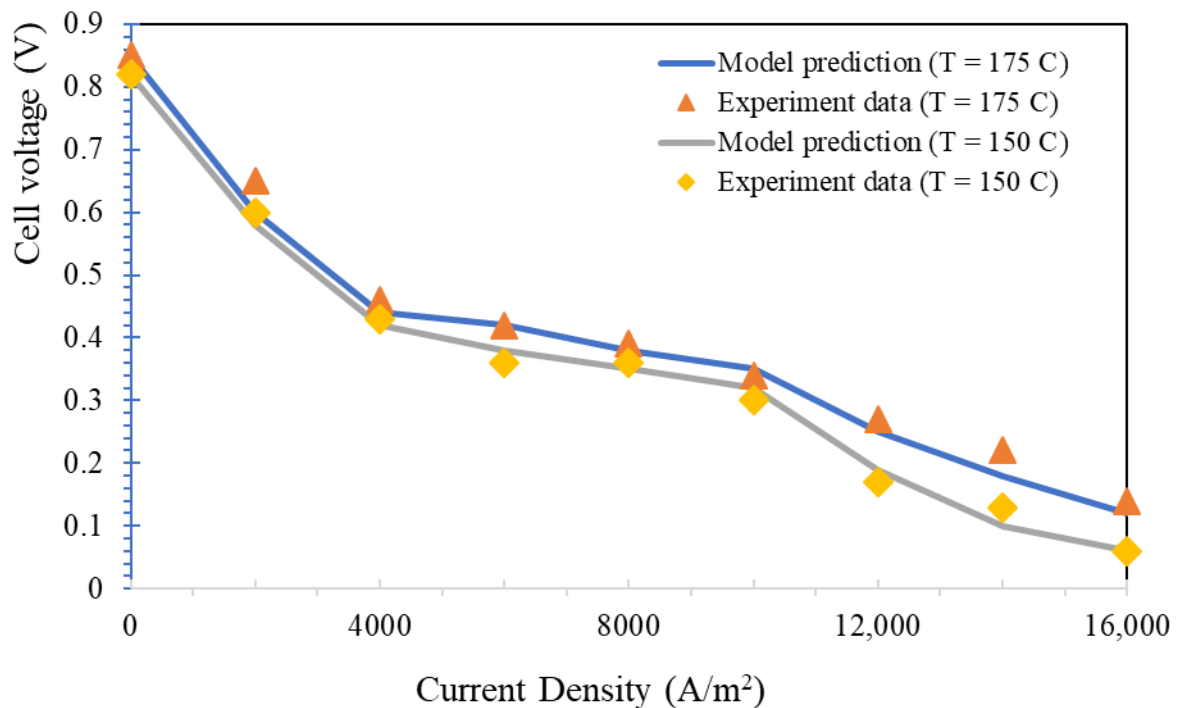


**Figure 3.** Validation of the HT-PEMFC voltage model with Sousa's model.

## 6. Results and Discussions

### 6.1. Thermodynamic Performance of the System

The target ship uses 3800 kW of electrical power to cover the needs of the main propulsion plant, auxiliary machinery, maneuvering regime, and the seafarers' demands. The SOFC fuel utilization factor and energy efficiency of the proposed system were computed to be 0.86 and 52%. After applying the aforementioned thermodynamic model to evaluate the system, it was determined that the integrated system's output power is 5650.86 kW. This amount of power is satisfactory to operate the ship and supply electricity for other applications. The energy and exergy efficiencies of the entire system were measured to be 77.51% and 44.71%, respectively. This is generated by seven different power sources, including four bottoming cycle turbines, gas turbines, and SOFC fuel cells. A total of 67.24% of the entire power output is generated by the SOFCs, whereas 32.67% is produced by the GT, PEMFCs, SRC, and the ORC subsystems, demonstrating that the waste heat recovery cycles operate the proposed system as expected.

The power generated by the major components is demonstrated in Figure 4.

Taking into account the entire system depicted in Figure 4 and Table 5, the SOFC-GT subsystem provided 4976 kW to the marine propulsion plant, accounting for 88% of the total power production.

**Table 5.** System's energy and exergy efficiencies.

Subsystem	Energy Efficiency	Exergy Efficiency
SOFC-GT	67.89	40.16
SRC	30.55	44.84
ORC	13.21	56.24
PEMFC-ORC	47.11	27.87
Total System	77.75	44.71

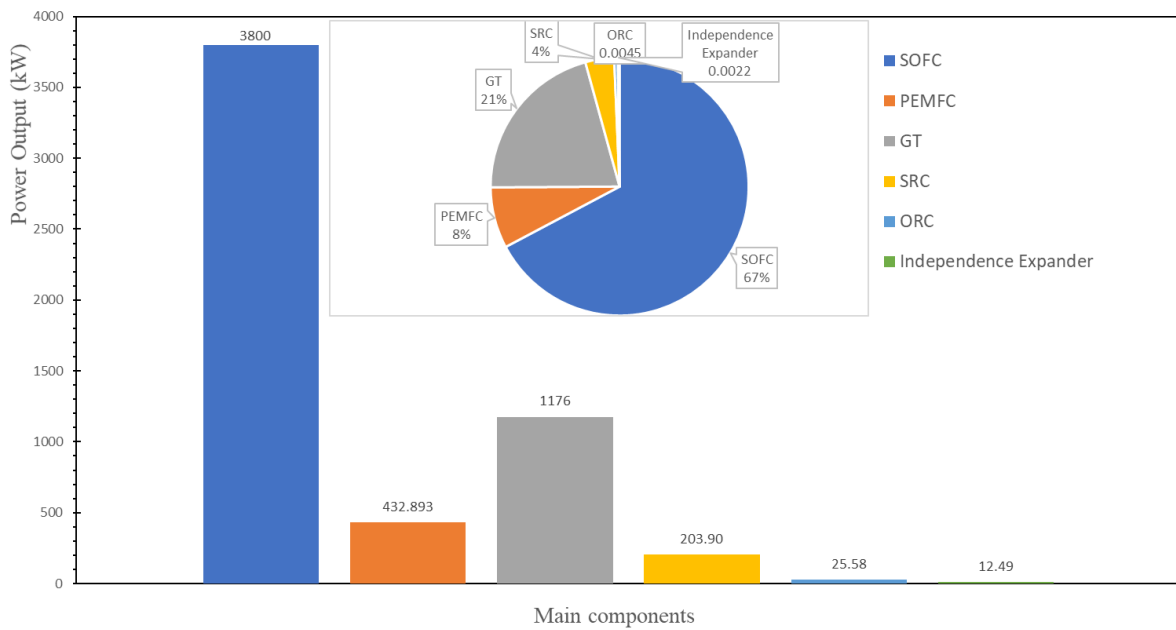


Figure 4. Power generated by the main components of the system.

It is interesting to recognize that the PEMFC-ORC system is more energetically efficient than the SRC. The energy and exergy efficiencies of PEMFC-ORC are estimated at 47.11% and 27.87%, respectively, whereas that of SRC was calculated to be 30.55% and 44.84%, respectively.

Figure 5 depicts an analysis of the exergy destruction connected to the internal thermal procedures that occur in the major system components. The largest exergy destruction belongs to SOFC, with 2721.34 kW, followed by GT, with 2405.68 kW. The large exergy loss suggests that the gas turbine has greater potential for improvement than the other machinery components. The third is the afterburner, which has an exergy destruction of 927.63 kW. Next are the PEMFCs, with an exergy destruction of 418.89 kW. The HEX-7 exhibits the lowest exergy destruction due to its greater entropy production at a constant heat transfer rate and low temperatures.

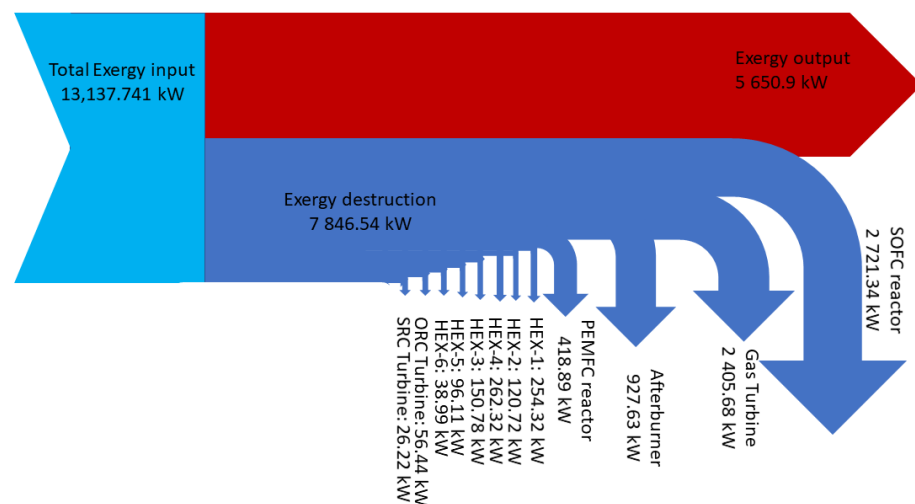


Figure 5. Exergy destruction presentation.

The thermodynamics properties of each node are depicted on Table 6.

**Table 6.** The thermodynamics properties of stated points.

	Vapor Fraction	Temperature	Pressure	Molar Flow	Liquid Volume Flow	Mass Enthalpy
Unit		°C	kPa	kgmole/h	m <sup>3</sup> /h	kJ/kg
Air in	1.00	25.00	101.30	424.71	14.16	−0.28
Water	0.00	25.00	100.00	64.70	1.17	−15,887.82
Methanol	0.00	22.20	101.32	36.50	1.47	−7558.71
1	0.00	22.23	400.00	36.50	1.47	−7558.27
2	0.00	30.00	393.11	36.50	1.47	−7531.06
3	1.00	250.00	389.66	36.50	1.47	−5921.80
4	1.00	249.52	389.66	174.20	5.62	−8535.20
5	1.00	249.85	389.66	101.37	2.89	−96.00
5-1	1.00	249.85	389.66	72.83	2.72	−9544.67
6	1.00	249.85	389.66	89.21	2.55	−96.00
7	1.00	249.85	389.66	12.16	0.35	−96.00
8	1.00	462.00	382.76	89.19	2.55	2470.70
9	1.00	28.00	140.00	152.90	5.10	2.65
10	1.00	507.65	382.76	540.25	17.56	530.20
11	1.00	882.68	382.76	526.99	16.90	530.20
12	1.00	882.68	382.76	500.64	16.05	530.20
12-1	1.00	882.68	382.76	26.35	0.84	530.20
13	1.00	1140.41	382.76	491.76	15.61	530.21
14	1.00	893.65	146.00	491.76	15.61	190.78
15	1.00	650.10	139.11	491.76	15.61	−133.44
16	1.00	615.75	104.63	491.76	15.61	−178.23
17	1.00	467.63	97.74	491.76	15.61	−368.40
18	1.00	250.59	90.84	491.76	15.61	−638.04
19	1.00	125.08	83.95	491.76	15.61	−788.94
20	0.00	25.03	420.00	64.70	1.17	−15,887.40
21	1.00	250.00	416.55	64.70	1.17	−13,002.16
22	1.00	186.36	400.00	424.71	14.16	165.47
23	1.00	492.60	396.55	424.71	14.16	495.48
24	0.00	71.41	19,000.00	56.62	1.02	−15,670.43
25	1.00	360.90	18,996.55	56.62	1.02	−13,345.07
26	0.69	74.69	38.00	56.62	1.02	−14,064.79
27	0.00	70.00	31.11	56.62	1.02	−15,693.37
28	0.00	20.00	100.00	444.07	8.02	−15,909.39
29	0.00	68.06	96.55	444.07	8.02	−15,701.75
30	1.00	122.39	120.00	12.16	0.35	−1598.22
31	1.00	165.77	120.00	172.37	5.66	−8.14
32	1.00	165.77	120.00	163.75	5.38	−8.14
33	1.00	165.77	120.00	8.62	0.28	−8.14
34	1.00	37.00	113.11	163.75	5.38	−149.08
35	1.00	30.27	78.63	163.75	5.38	−156.25
36	0.00	34.25	3045.00	28.00	2.79	−6731.67
37	1.00	115.00	3010.53	28.00	2.79	−6567.87
38	0.96	34.92	480.00	28.00	2.79	−6591.97
39	0.00	32.00	445.53	28.00	2.79	−6734.13
40	0.00	22.00	100.00	800.00	14.44	−15,900.76
41	0.00	30.74	93.11	800.00	14.44	−15,863.07

## 6.2. Parametric Study

The first and second laws of thermodynamics were used for parametric investigations to assess the integrated system's overall performance. The parametric study examined how the varying current density of the SOFCs would affect the efficiency of the overall system. The effect of the hydrogen distribution ratios was implemented.

### 6.2.1. Effect of $\beta$ -parameter

The  $\beta$ -parameter is the ratio of the hydrogen (separated by the PSA unit) to the total amount of hydrogen entering the PEMFCs. In the base case for the simulation, the  $\beta$  was

set at 0.12, which is sufficient to support the PEMFCs system and provide 423.893 kW of power output for the entire system. As the  $\beta$  ratio increases from 0 to 0.4, the total efficiency of the systems decreased accordingly. The change in the power output from the PEMFCs and other main power generation components of the system, according to different values of  $\beta$ -parameter, are presented in Figure 6.

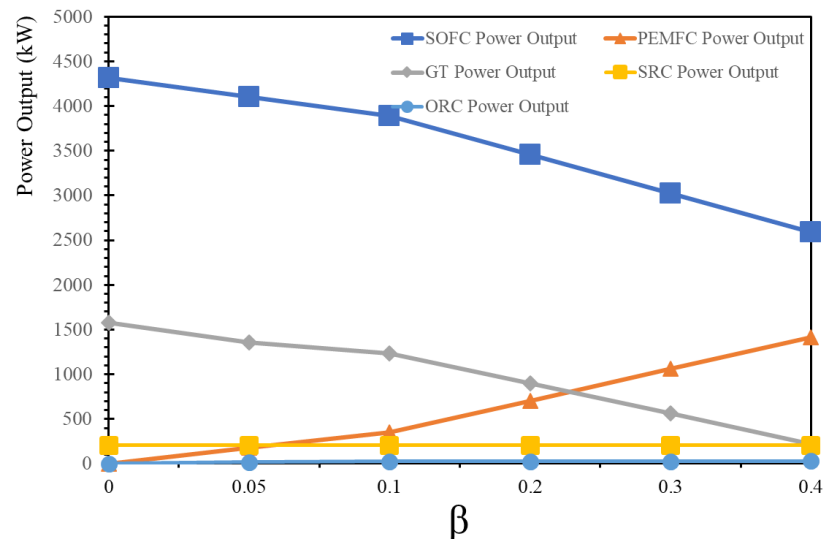


**Figure 6.** Influence of  $\beta$ -parameter on the power output of the system.

From Figure 6, the SOFC power decreased from 4319.36 to 2591.61 kW, whereas the PEMFC output power increased from 0 to 1415.382 kW when the  $\beta$ -parameter varied from 0 to 0.4. This can be explained by the increasing hydrogen flow rate to the PEMFCs and decreasing hydrogen flow rate to the SOFCs. This also resulted in the modification of the components and systems for waste heat usage in accordance with the SOFCs and PEMFCs. The larger the reduction in SOFC exhaust gases, the lower the power output of the GT and SRC, and vice versa. These modifications altered the energy and exergy efficiency of the components and systems, as shown in Figures 7 and 8.

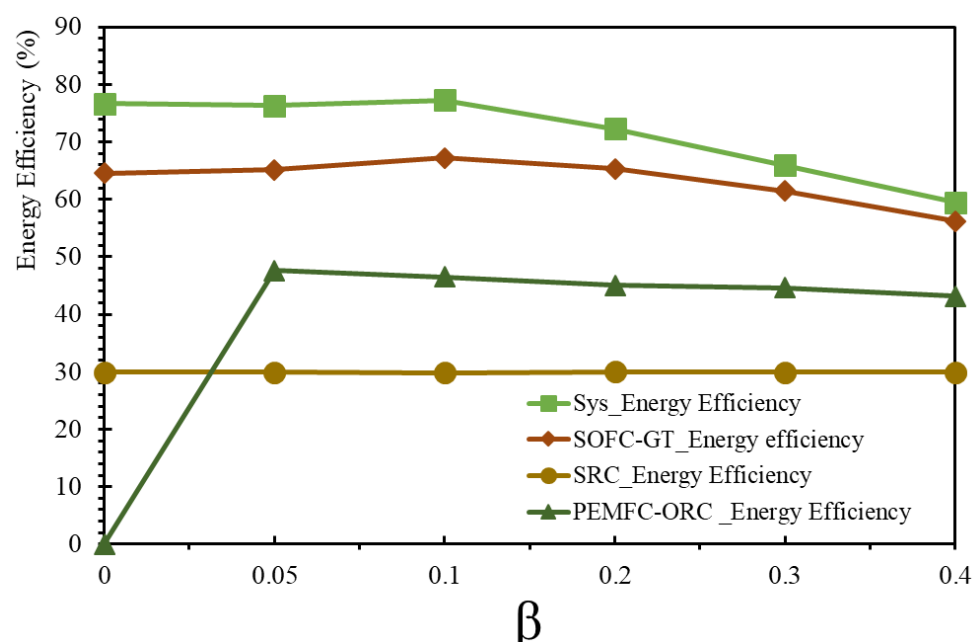


**Figure 7.** Influence of  $\beta$ -parameter on the energy efficiency of the system.

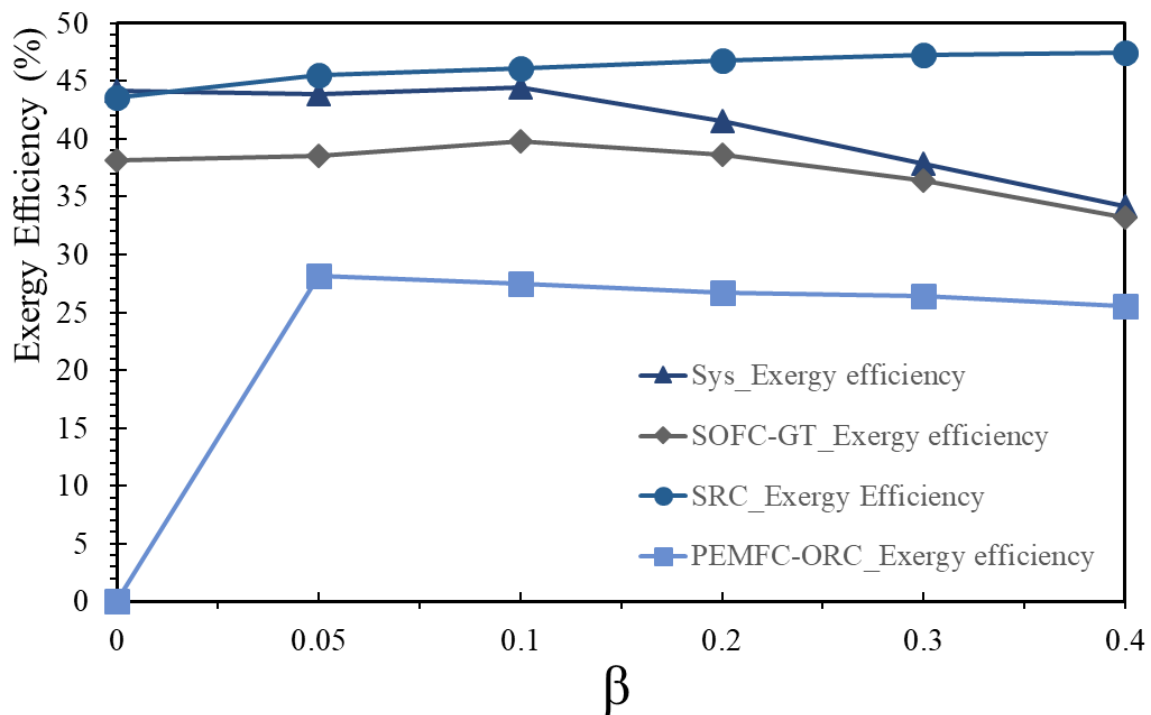


**Figure 8.** Influence of  $\beta$ -parameter on the system's exergy efficiency.

Energetically, the energy efficiency of the system decreases slightly as  $\beta$ -parameter increases. This is due to the effect of decreasing the device output power, particularly that of the SOFCs and the GT, as presented in Figure 6. However, the exergy of some components increased with an increasing  $\beta$ -parameter, as presented in Figure 8. With an increase in  $\beta$  from 0 to 0.4, the exergy of SRC increased from 43.6% to 47.47%, whereas the exergy efficiency of the PEMFCs slightly reduced from 28.15% to 25.53%.

#### 6.2.2. Influence of Current Density on SOFC

The performance of the fuel cell and the system are largely influenced by the current density. Figure 9 depicts how current density influences the essential components and the system's efficiency. This graph displays current densities, ranging from 900 to 1800 A/m<sup>2</sup>. The SOFCs voltage reduces with rising current density, and SOFC efficiency also decreases. At 900 A/m<sup>2</sup>, the net electrical cycle efficiency was 86.01%, whereas it was 56.01% at 1800 A/m<sup>2</sup>. As current density increased, the SOFC-energy GTs efficiency decreased from 66.87% to 60.82%. This is primarily the result of raising the mass flow rate from 193.1 to 320.5 kg·h<sup>-1</sup> in order to keep a predetermined output power for the SOFCs. In contrast, the heating cogeneration efficiency of SRC ranged from 29.87% (at 900 A/m<sup>2</sup> of current density) to 30.02% (at 1800 A/m<sup>2</sup> of current density). The lowest efficiency gain of the trigeneration cycle was also substantial at 32.21%, when measured against net electrical efficiency. The energy efficiency of the PEMFC-ORC varied from 39.38% to 44.18% as the current density increased. It is also intriguing that variations in the current density appear to have a minor effect on subsystem's energy efficiency.

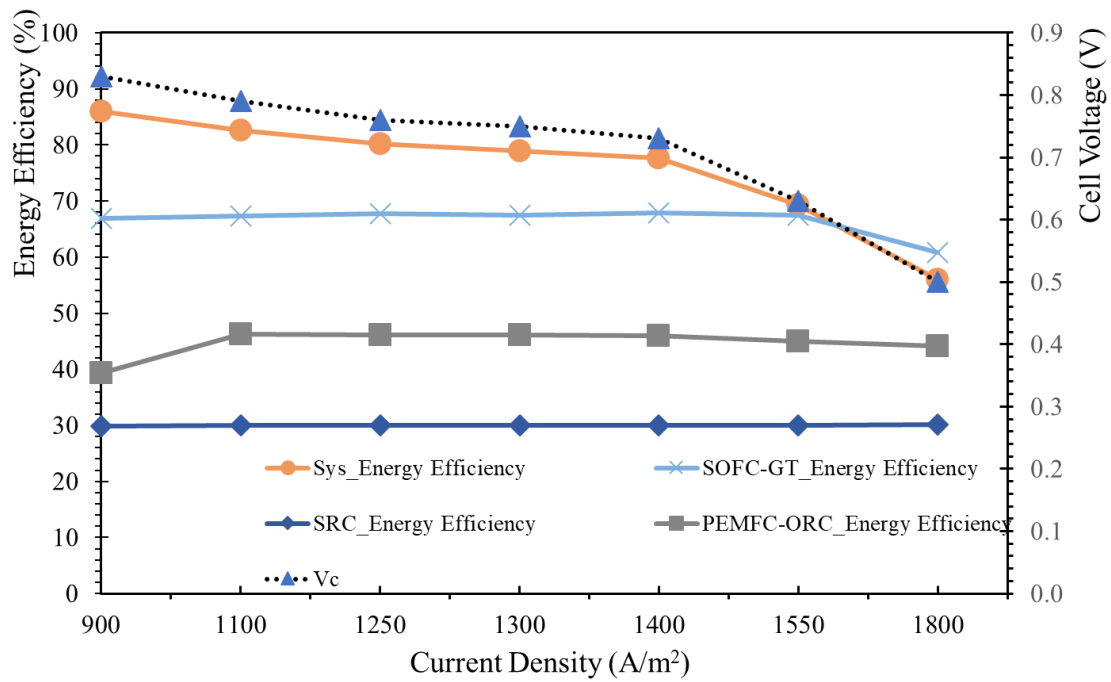


Figure 9. Energy efficiency response to variations in current density.

Figure 10 depicts the exergy efficiency response of the system to a variety of current densities. Due to the effect of a reduction in cell voltage ( $V_c$ ) during an increase in current density, it was discovered that the efficiency of the combined system decreased, whereas the total power output increased. The exergy efficiency reduced from 49.47% to 32.21% for the measured range of current densities.

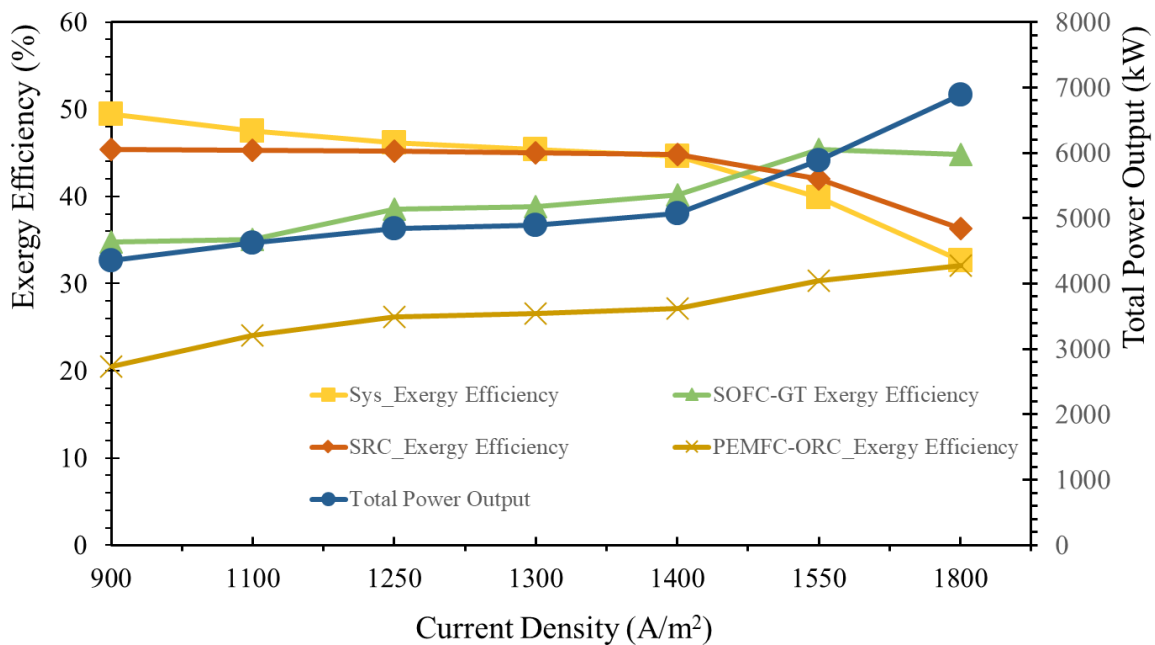
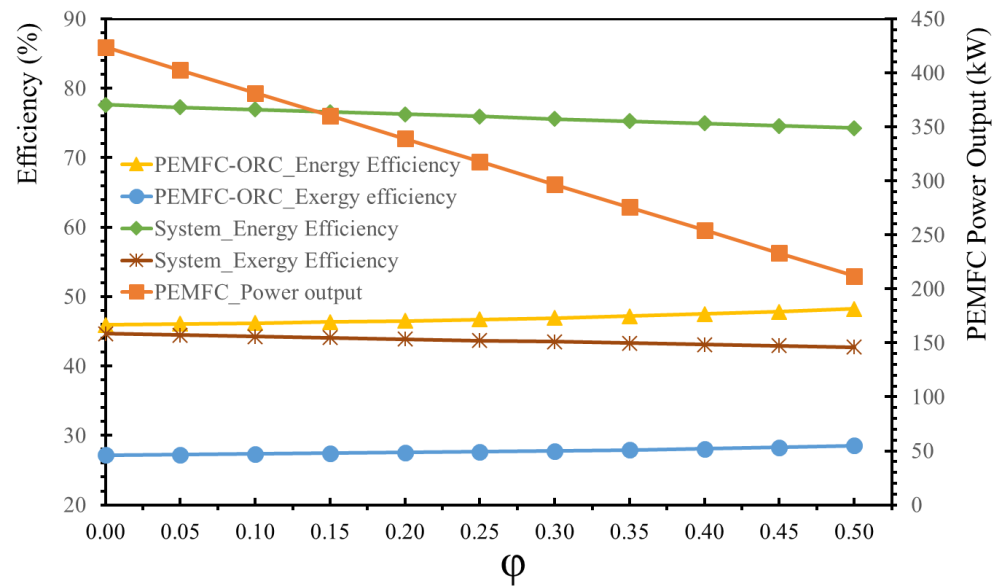


Figure 10. Responses of system's exergy efficiency to variations in current density.

### 6.2.3. Effect of the $\varphi$ -Parameter

The  $\varphi$ -parameter is defined as the rate of hydrogen to the storage tank (stream 30-2) and the total amount of hydrogen supplied to the PEMFC system (stream 30). As the ratio ranged from 0–0.5, the efficiency of the PEMFC-ORC subsystem and the entire system is

illustrated in Figure 11 below. The efficiency of the PEMFC-ORC increased in line with the amount of hydrogen supplied to the H<sub>2</sub> tank (stream 30-2). However, the higher  $\varphi$  value indicates a hydrogen reduction in the PEMFC. If the  $\varphi$ -parameter increases from 0–0.5, the power output of the PEMFCs will decrease from 423.89 to 211.95 kW. This reduces the total energy efficiency of the system by 3.34%, from 77.61% to 74.27%. It is important to note that, during the maneuvering and starting up phases of a vessel, a rapid power response is required. Thus, the PEMFCs and their hydrogen storage system is an excellent solution for systems with immediate power demands.



**Figure 11.** Influence of  $\varphi$ -Parameter on the system efficiency.

As a result, a crucial component of the PEMFC-ORC system, which is designed to handle the operational behavior of the combined systems, is the ability to enhance the energy efficiency of the PEMFCs. The exergy efficiency is 18.77% greater than the energy efficiency, and the growth patterns of both subsystems are linear. This demonstrates that this component can generate electric power, the primary output required to drive the propulsion plant of the vessel in question.

#### 6.2.4. Working Fluid for ORC

When harvesting waste energy from the cooling oil of the HT-PEMFCs, the expander device (of the ORC) is designed to transfer heat into useful energy. The output power and ORC efficiency are greatly affected by the quality of the organic fluid. The ORC cycle's effectiveness was improved by the selection of the organic fluid. In this study, the working fluid candidates, R134a, R124, R152a, R600, and R601, were evaluated. The characteristics of the potential organic fluids are demonstrated in Table 7.

**Table 7.** Characteristics of the working fluids.

Working Fluid	ODP	GWP	Molecular Mass (g/mol)	Safety Class (ASHRAE 34)	Boiling Temperature [°C]	Critical Temp.		Critical Pressure [kPa]
						[°C]	[kPa]	
R124	0.02	609	136.48	A1	−11	122.4	3624	
R134a	0	1320	102.03	A1	−26.1	101.1	4059	
R600	0	20	58.13	A3	−0.55	151.98	3796	
R152a	0	124	66.04	A2	−14.0	113.0	4517	
R601	0	20	72.15	A3	36.0	187.55	3390	

As shown in Table 7, the R124 properties are ideally suited for the target system, with an output temperature of 165.8 °C and a mass flow rate of 4441 kg/h. In addition, as this system is intended for marine vessels, the working fluid was carefully considered according to classification societies (for shipping references), such as the American Society of Heating, Refrigerating and Air-Conditioning Engineers (ASHARE 34) [75] and the Korea Register of Shipping (KR) [76].

Using R124 as the desired fluid, a case study was performed to determine how the net power output, energy, and exergy efficiencies of an ORC would respond to a variety of superheated temperatures (in the organic fluids). Stream 32 is the hot source stream, with a pressure and temperature of 165.8 °C and 120 kPa. Thus, the range of the superheated fluid temperatures was between 100 and 140 °C. Figure 12 depicts the response of system performance to the superheated temperature.

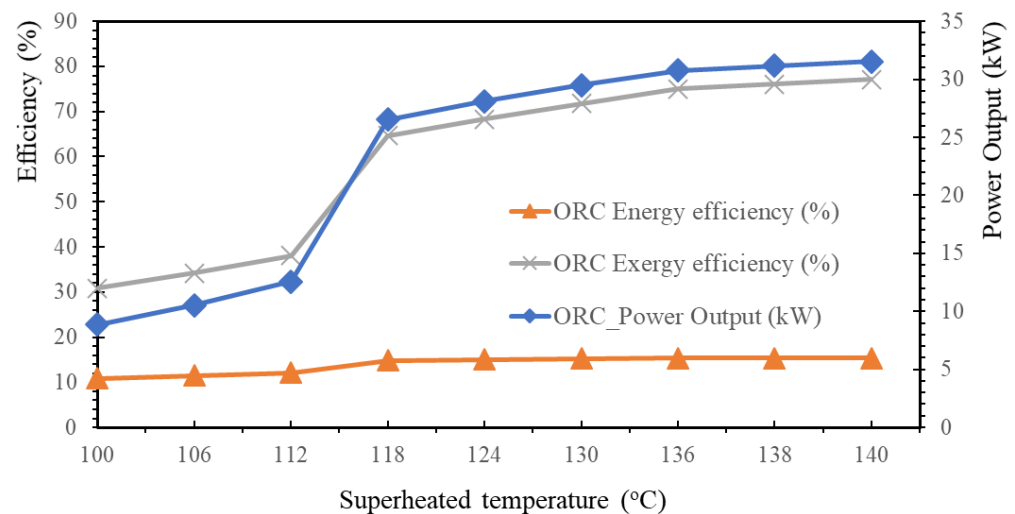


**Figure 12.** Influence of ORC system performance from the superheated temperature of R124.

The output power of the system increased from 8.871 to 31.15 kW, and its energy efficiency increased from 10.84% to 15.38% as the superheated temperature increased from 100–140 °C. However, the increasing trend decreases with an increase in the superheated temperature. This is because the PEMFCs cooling system's hot source has been fixed. Consequently, the influence of log means that the influence of the temperature on the operational effectiveness of HEX-7 is distinct. Otherwise, according to the properties of an organic fluid, lowering the superheated temperature may result in the formation of liquid at the turbine's input, which may cause damage to the system.

## 7. Conclusions

A system that integrates SOFC-SRC-PEMFC-ORC, using methanol as the main fuel to generate electricity for the marine primary propulsion system and harvest high-temperature exhaust heat from SOFCs to produce additional electric power for the start-up and maneuvering regime of a ship, as well as the accommodation of seafarers, was proposed and investigated. By utilizing renewable, sulfur-free, and low-carbon fuels in the power plant, the goal of the planned multigenerational system was to supply a marine vessel with an alternative sustainability solution. Energy and exergy assessments, as well as an extensive parametric analysis, were carried out to evaluate the proposed system's functionality and energy harvesting. Among the most important findings of this study are the following.

- ① This study proposed a novel integrated system for marine vessel application to overcome the primary barrier of SOFC application during start-up and maneuvering. The total efficiency of the energy and exergy of the integrated system was calculated to be 77.75% and 44.71%, respectively, which is significantly higher than that of SOFC stand-alone systems. The SRC-PEMFC-ORC produced and supplied 1850.86 kW to

the system, representing 32.75% of the system's total power supply. This system also produced hot water for the sailors onboard the ship;

- ② The parametric studies showed that the energy and exergy efficiencies of the entire system decreased by 30% and 17.26%, respectively, with an increase in current density from 900 to 1800 A/m<sup>2</sup>. However, the overall power output of the cogeneration system increased by 2258.5 kW in the tested range of the current density;
- ③ By varying the distribution ratio ( $\beta$ ) from 0 to 0.4, the SOFC power decreased from 4319.36 to 2591.61 kW, whereas the PEMFCs output power increased from 0 to 1415.382 kW. The exergy efficiency of the PEMFCs slightly reduced from 28.15% to 25.53%;
- ④ When the  $\varphi$ -parameter was expanded from 0 to 0.5, the output power of the PEMFCs decreased from 423.89 to 211.95 kW. This reduction makes the total energy efficiency of the system decrease by 3.34%, from 77.61% to 74.27%.

These findings indicate that the innovation of high-efficiency SOFC-GT-SRC-PEMFC-ORC maritime propulsion systems using methanol as a fuel is promising. In order to thoroughly comprehend the applicability of the aforementioned combination system, future research on the evaluation of the system's economic and sustainability aspects has been planned. Future research should also investigate the system's dynamic behavior, given that this combined system is suggested for further applications involving marine vessels.

**Author Contributions:** Formal analysis, P.A.D.; Investigation, B.R.; Methodology, P.A.D.; Supervision, H.K. and J.J.; Writing—original draft, P.A.D.; Writing—review and editing, H.K. and P.A.D. All authors have read and agreed to the published version of the manuscript.

**Funding:** This research was supported by the Korea Evaluation Institute of Industrial Technology (KEIT) grant funded by the Korea Government (MOTIE) (RS-2022-00144116). This research was supported by the Korea Institute of Marine Science & Technology Promotion (KIMST), funded by the Ministry of Oceans and Fisheries, Korea (20200520, 20220440). This research was supported by BB21plus, funded by the Busan Metropolitan City and Busan Institute for Talent and Lifelong Education (BIT).

**Institutional Review Board Statement:** Not applicable.

**Informed Consent Statement:** Not applicable.

**Data Availability Statement:** Not applicable.

**Conflicts of Interest:** The authors declare no conflict of interest.

## Nomenclature

$A$	Active surface area, m <sup>2</sup>	LHV	Lower heating value, kJ/kg
AC	Alternative current	$M$	Relative molecular mass (kg/mol)
CV	Control volume	MSE	Carbon mass specific emission
DC	Direct current	$\dot{m}_{CO}$	Mass flow rate of CO (kg/h)
$\dot{E}x_{dest}$	Exergy destruction rate, kW	$m$	Mass flow rate, kg/h
$ex$	Specific exergy, kJ/kg	$P$	Pressure, bar
$F$	Faraday constant, 96.458 C/mole	PR	Peng–Robinson
$G$	Gibbs free energy, kJ/kg	$\dot{Q}$	Heat transfer rate, kW
$\dot{G}$	Molar Gibbs free energy (kJ/kmol)	$T$	Temperature, °C or K
$g$	The mass fraction	$V_c$	Actual voltage of stack, V
HEX	Heat exchanger	$V_{ohm}$	Ohmic voltage losses, V
$h$	Specific enthalpy, kJ/kg	$V_R$	Cell ideal reversible voltage, V
$I$	Current (A)	$V_{act}$	Activation voltage loss, V
$i$	Current density, A/m <sup>2</sup>	$\dot{W}$	Net electric power, kW

Greek letters			
$\beta$	Distribution ratio of hydrogen	$\gamma$	Adiabatic coefficient
$\eta_{DA}$	Efficiency of the inverter, %	$\varphi$	Ratio of hydrogen to storage tank
$\lambda$	Stoichiometry		
Acronyms			
GT	Gas Turbine	PEMFC	Proton-exchange membrane fuel cells
HT-PEMFC	High temperature Proton-exchange membrane fuel cells	PSA	Pressure Swing Adsorption
LT-PEMFC	Low temperature Proton-exchange membrane fuel cells	ORC	Organic Rankine Cycle
MRS	Methanol Reforming system	SOFC	Solid oxide fuel cells
		SRC	Steam Rankine Cycle

## References

- Zis, T.P.; Psaraftis, H.N.; Tillig, F.; Ringsberg, J.W. Decarbonizing maritime transport: A Ro-Pax case study. *Res. Transp. Bus. Manag.* **2020**, *37*, 100565. [\[CrossRef\]](#)
- Li, R.; Liu, Y.; Wang, Q. Emissions in maritime transport: A decomposition analysis from the perspective of production-based and consumption-based emissions. *Mar. Policy* **2022**, *143*, 105125. [\[CrossRef\]](#)
- Xing, H.; Stuart, C.; Spence, S.; Chen, H. Alternative fuel options for low carbon maritime transportation: Pathways to 2050. *J. Clean. Prod.* **2021**, *297*, 126651. [\[CrossRef\]](#)
- Al-Enazi, A.; Okonkwo, E.C.; Bicer, Y.; Al-Ansari, T. A review of cleaner alternative fuels for maritime transportation. *Energy Rep.* **2021**, *7*, 1962–1985. [\[CrossRef\]](#)
- The International Maritime Organization. *Resolution MPEC.328(76)*; IMO: London, UK, 2021; Volume MPEC 76/15, pp. 37–72.
- International Maritime Organization. *Adoption of the Initial IMO Strategy on Reduction of GHG Emissions from Ships*; IMO: London, UK, 2018; Volume 10.
- Hansson, J.; Brynolf, S.; Fridell, E.; Lehtveer, M. The Potential Role of Ammonia as Marine Fuel—Based on Energy Systems Modeling and Multi-Criteria Decision Analysis. *Sustainability* **2020**, *12*, 3265. [\[CrossRef\]](#)
- Sürer, M.G.; Arat, H.T. Advancements and current technologies on hydrogen fuel cell applications for marine vehicles. *Int. J. Hydrog. Energy* **2022**, *47*, 19865–19875. [\[CrossRef\]](#)
- Alkhaledi, A.N.; Sampath, S.; Pilidis, P. Propulsion of a hydrogen-fuelled LH2 tanker ship. *Int. J. Hydrog. Energy* **2022**, *47*, 17407–17422. [\[CrossRef\]](#)
- Li, H.; Ma, C.; Zou, X.; Li, A.; Huang, Z.; Zhu, L. On-board methanol catalytic reforming for hydrogen Production-A review. *Int. J. Hydrog. Energy* **2021**, *46*, 22303–22327. [\[CrossRef\]](#)
- Valera-Medina, A.; Amer-Hatem, F.; Azad, A.K.; Dedoussi, I.C.; de Joannon, M.; Fernandes, R.X.; Glarborg, P.; Hashemi, H.; He, X.; Mashruk, S.; et al. Review on Ammonia as a Potential Fuel: From Synthesis to Economics. *Energy Fuels* **2021**, *35*, 6964–7029. [\[CrossRef\]](#)
- Adamson, K.-A.; Pearson, P. Hydrogen and methanol: A comparison of safety, economics, efficiencies and emissions. *J. Power Sources* **2000**, *86*, 548–555. [\[CrossRef\]](#)
- Wang, C.; Li, Y.; Xu, C.; Badawy, T.; Sahu, A.; Jiang, C. Methanol as an octane booster for gasoline fuels. *Fuel* **2019**, *248*, 76–84. [\[CrossRef\]](#)
- Kulikovsky, A. Optimal temperature for DMFC stack operation. *Electrochim. Acta* **2008**, *53*, 6391–6396. [\[CrossRef\]](#)
- Atacan, O.; Ouellette, D.; Colpan, C. Two-dimensional multiphase non-isothermal modeling of a flowing electrolyte—Direct methanol fuel cell. *Int. J. Hydrog. Energy* **2017**, *42*, 2669–2679. [\[CrossRef\]](#)
- Calabriso, A.; Cedola, L.; Del Zotto, L.; Rispoli, F.; Santori, S.G. Performance investigation of Passive Direct Methanol Fuel Cell in different structural configurations. *J. Clean. Prod.* **2015**, *88*, 23–28. [\[CrossRef\]](#)
- Alias, M.; Kamarudin, S.; Zainoodin, A.; Masdar, M. Active direct methanol fuel cell: An overview. *Int. J. Hydrog. Energy* **2020**, *45*, 19620–19641. [\[CrossRef\]](#)
- Zhao, J.; Cai, S.; Luo, X.; Tu, Z. Dynamic characteristics and economic analysis of PEMFC-based CCHP systems with different dehumidification solutions. *Int. J. Hydrog. Energy* **2022**, *47*, 11644–11657. [\[CrossRef\]](#)
- Perng, S.-W.; Wu, H.-W. Influence of inlet-nozzle and outlet-diffuser mounted in the plate-shape reactor on PEMFC net power output and methanol steam reforming performance. *Appl. Energy* **2022**, *323*, 119510. [\[CrossRef\]](#)
- Chen, X.; Zhou, H.; Yu, Z.; Li, W.; Tang, J.; Xu, C.; Ding, Y.; Wan, Z. Thermodynamic and economic assessment of a PEMFC-based micro-CCHP system integrated with geothermal-assisted methanol reforming. *Int. J. Hydrog. Energy* **2020**, *45*, 958–971. [\[CrossRef\]](#)
- Özcan, O.; Akin, A.N. Thermodynamic analysis of methanol steam reforming to produce hydrogen for HT-PEMFC: An optimization study. *Int. J. Hydrog. Energy* **2019**, *44*, 14117–14126. [\[CrossRef\]](#)
- Sankar, K.; Thakre, N.; Singh, S.M.; Jana, A.K. Sliding mode observer based nonlinear control of a PEMFC integrated with a methanol reformer. *Energy* **2017**, *139*, 1126–1143. [\[CrossRef\]](#)

23. Chen, C.-C.; Jeng, M.-S.; Leu, C.-H.; Yang, C.-C.; Lin, Y.-L.; King, S.-C.; Wu, S.-Y. Low-level CO in hydrogen-rich gas supplied by a methanol processor for PEMFCs. *Chem. Eng. Sci.* **2011**, *66*, 5095–5106. [[CrossRef](#)]
24. Kim, T.; Ahn, K.; Vohs, J.M.; Gorte, R.J. Deactivation of ceria-based SOFC anodes in methanol. *J. Power Sources* **2007**, *164*, 42–48. [[CrossRef](#)]
25. Bicer, Y.; Khalid, F. Life cycle environmental impact comparison of solid oxide fuel cells fueled by natural gas, hydrogen, ammonia and methanol for combined heat and power generation. *Int. J. Hydrog. Energy* **2018**, *45*, 3670–3685. [[CrossRef](#)]
26. Laosiripojana, N.; Assabumrungrat, S. The effect of specific surface area on the activity of nano-scale ceria catalysts for methanol decomposition with and without steam at SOFC operating temperatures. *Chem. Eng. Sci.* **2006**, *61*, 2540–2549. [[CrossRef](#)]
27. Haseltalab, A.; van Biert, L.; Sapra, H.; Mestemaker, B.; Negenborn, R.R. Component sizing and energy management for SOFC-based ship power systems. *Energy Convers. Manag.* **2021**, *245*, 114625. [[CrossRef](#)]
28. Xu, Q.; Xia, L.; He, Q.; Guo, Z.; Ni, M. Thermo-electrochemical modelling of high temperature methanol-fuelled solid oxide fuel cells. *Appl. Energy* **2021**, *291*, 116832. [[CrossRef](#)]
29. Zhou, J.; Wang, Z.; Han, M.; Sun, Z.; Sun, K. Optimization of a 30 kW SOFC combined heat and power system with different cycles and hydrocarbon fuels. *Int. J. Hydrog. Energy* **2021**, *47*, 4109–4119. [[CrossRef](#)]
30. Zhang, Y.; Huang, Z.; Gan, T.; Hou, N.; Fan, L.; Zhou, X.; Gao, G.; Li, J.; Zhao, Y.; Li, Y. Cu-Ce<sub>0.8</sub>Sm<sub>0.2</sub>O<sub>2-δ</sub> anode for electrochemical oxidation of methanol in solid oxide fuel cell: Improved activity by La and Nd doping. *Solid State Ionics* **2021**, *369*, 115728. [[CrossRef](#)]
31. Duong, P.A.; Ryu, B.; Kim, C.; Lee, J.; Kang, H. Energy and Exergy Analysis of an Ammonia Fuel Cell Integrated System for Marine Vessels. *Energies* **2022**, *15*, 3331. [[CrossRef](#)]
32. Herdem, M.S.; Farhad, S.; Hamdullahpur, F. Modeling and parametric study of a methanol reformat gas-fueled HT-PEMFC system for portable power generation applications. *Energy Convers. Manag.* **2015**, *101*, 19–29. [[CrossRef](#)]
33. Wang, S. Exergy analysis and optimization of methanol generating hydrogen system for PEMFC. *Int. J. Hydrog. Energy* **2006**, *31*, 1747–1755. [[CrossRef](#)]
34. Bepari, S.; Kuila, D. Steam reforming of methanol, ethanol and glycerol over nickel-based catalysts-A review. *Int. J. Hydrog. Energy* **2019**, *45*, 18090–18113. [[CrossRef](#)]
35. Al-Hamed, K.H.; Dincer, I. A novel ammonia solid oxide fuel cell-based powering system with on-board hydrogen production for clean locomotives. *Energy* **2021**, *220*, 119771. [[CrossRef](#)]
36. Yilmaz, F.; Ozturk, M. Design and modeling of an integrated combined plant with SOFC for hydrogen and ammonia generation. *Int. J. Hydrog. Energy* **2022**, *47*, 31911–31926. [[CrossRef](#)]
37. Al-Hamed, K.; Dincer, I. A new direct ammonia solid oxide fuel cell and gas turbine based integrated system for electric rail transportation. *eTransportation* **2019**, *2*, 100027. [[CrossRef](#)]
38. Purnama, H.; Girgsdies, F.; Ressler, T.; Schattka, J.; Caruso, R.; Schomäcker, R.; Schlögl, R. Activity and Selectivity of a Nanostructured CuO/ZrO<sub>2</sub> Catalyst in the Steam Reforming of Methanol. *Catal. Lett.* **2004**, *94*, 61–68. [[CrossRef](#)]
39. Faungnawakij, K.; Kikuchi, R.; Eguchi, K. Thermodynamic evaluation of methanol steam reforming for hydrogen production. *J. Power Sources* **2006**, *161*, 87–94. [[CrossRef](#)]
40. Jjagwe, J.; Olupot, P.W.; Menya, E.; Kalibbala, H.M. Synthesis and Application of Granular Activated Carbon from Biomass Waste Materials for Water Treatment: A Review. *J. Bioresour. Bioprod.* **2021**, *6*, 292–322. [[CrossRef](#)]
41. Sarabchi, N.; Mahmoudi, S.S.; Yari, M.; Farzi, A. Exergoeconomic analysis and optimization of a novel hybrid cogeneration system: High-temperature proton exchange membrane fuel cell/Kalina cycle, driven by solar energy. *Energy Convers. Manag.* **2019**, *190*, 14–33. [[CrossRef](#)]
42. Ishak, F.; Dincer, I.; Zamfirescu, C. Energy and exergy analyses of direct ammonia solid oxide fuel cell integrated with gas turbine power cycle. *J. Power Sources* **2012**, *212*, 73–85. [[CrossRef](#)]
43. Rathore, S.S.; Biswas, S.; Fini, D.; Kulkarni, A.P.; Giddey, S. Direct ammonia solid-oxide fuel cells: A review of progress and prospects. *Int. J. Hydrog. Energy* **2021**, *46*, 35365–35384. [[CrossRef](#)]
44. Ishak, F.; Dincer, I.; Zamfirescu, C. Thermodynamic analysis of ammonia-fed solid oxide fuel cells. *J. Power Sources* **2011**, *202*, 157–165. [[CrossRef](#)]
45. Authayanun, S.; Mamlouk, M.; Arpornwichanop, A. Maximizing the efficiency of a HT-PEMFC system integrated with glycerol reformer. *Int. J. Hydrog. Energy* **2012**, *37*, 6808–6817. [[CrossRef](#)]
46. Siddiqui, O.; Dincer, I. A review and comparative assessment of direct ammonia fuel cells. *Therm. Sci. Eng. Prog.* **2018**, *5*, 568–578. [[CrossRef](#)]
47. Song, M.; Zhuang, Y.; Zhang, L.; Li, W.; Du, J.; Shen, S. Thermodynamic performance assessment of SOFC-RC-KC system for multiple waste heat recovery. *Energy Convers. Manag.* **2021**, *245*, 114579. [[CrossRef](#)]
48. Liu, Y.; Han, J.; You, H. Performance analysis of a CCHP system based on SOFC/GT/CO<sub>2</sub> cycle and ORC with LNG cold energy utilization. *Int. J. Hydrog. Energy* **2019**, *44*, 29700–29710. [[CrossRef](#)]
49. Chitgar, N.; Moghimi, M. Design and evaluation of a novel multi-generation system based on SOFC-GT for electricity, fresh water and hydrogen production. *Energy* **2020**, *197*, 117162. [[CrossRef](#)]
50. Ezzat, M.; Dincer, I. Energy and exergy analyses of a novel ammonia combined power plant operating with gas turbine and solid oxide fuel cell systems. *Energy* **2019**, *194*, 116750. [[CrossRef](#)]

51. Fuerte, A.; Valenzuela, R.; Escudero, M.; Daza, L. Ammonia as efficient fuel for SOFC. *J. Power Sources* **2009**, *192*, 170–174. [[CrossRef](#)]
52. Ma, Q.; Peng, R.; Tian, L.; Meng, G. Direct utilization of ammonia in intermediate-temperature solid oxide fuel cells. *Electrochem. Commun.* **2006**, *8*, 1791–1795. [[CrossRef](#)]
53. Perna, A.; Minutillo, M.; Jannelli, E.; Cigolotti, V.; Nam, S.; Han, J. Design and performance assessment of a combined heat, hydrogen and power (CHHP) system based on ammonia-fueled SOFC. *Appl. Energy* **2018**, *231*, 1216–1229. [[CrossRef](#)]
54. Amiri, T.; Singh, K.; Sandhu, N.K.; Hanifi, A.R.; Etsell, T.H.; Luo, J.-L.; Thangadurai, V.; Sarkar, P. High Performance Tubular Solid Oxide Fuel Cell Based on  $\text{Ba}_{0.5}\text{Sr}_{0.5}\text{Ce}_{0.6}\text{Zr}_{0.2}\text{Gd}_{0.1}\text{Y}_{0.1}\text{O}_{3-\delta}$  Proton Conducting Electrolyte. *J. Electrochem. Soc.* **2018**, *165*, F764–F769. [[CrossRef](#)]
55. Milewski, J.; Szczeniński, A.; Szabłowski, Ł. A proton conducting solid oxide fuel cell—implementation of the reduced order model in available software and verification based on experimental data. *J. Power Sources* **2021**, *502*, 229948. [[CrossRef](#)]
56. Mehrpooya, M.; Dehghani, H.; Moosavian, S.A. Optimal design of solid oxide fuel cell, ammonia-water single effect absorption cycle and Rankine steam cycle hybrid system. *J. Power Sources* **2016**, *306*, 107–123. [[CrossRef](#)]
57. Han, J.; Han, J.; Yu, S. Investigation of FCVs durability under driving cycles using a model-based approach. *J. Energy Storage* **2020**, *27*, 101169. [[CrossRef](#)]
58. Chen, H.; Liu, Z.; Ye, X.; Yi, L.; Xu, S.; Zhang, T. Air flow and pressure optimization for air supply in proton exchange membrane fuel cell system. *Energy* **2021**, *238*, 121949. [[CrossRef](#)]
59. Dimitrova, Z.; Nader, W.B. PEM fuel cell as an auxiliary power unit for range extended hybrid electric vehicles. *Energy* **2021**, *239*, 121933. [[CrossRef](#)]
60. Smith, J.D.; Novy, M. Design of a Modern Proton-Exchange Membrane Fuel Cell Module for Engineering Education. In Proceedings of the 2018 IEEE Conference on Technologies for Sustainability (SusTech), Long Beach, CA, USA, 11–13 November 2018. [[CrossRef](#)]
61. Nalbant, Y.; Colpan, C.O.; Devrim, Y. Energy and exergy performance assessments of a high temperature-proton exchange membrane fuel cell based integrated cogeneration system. *Int. J. Hydrog. Energy* **2019**, *45*, 3584–3594. [[CrossRef](#)]
62. Rosli, R.; Sulong, A.; Daud, W.W.; Zulkifley, M.; Rosli, M.; Majlan, E.; Haque, M.; Radzuan, N.M. The design and development of an HT-PEMFC test cell and test station. *Int. J. Hydrog. Energy* **2019**, *44*, 30763–30771. [[CrossRef](#)]
63. Zhang, C.; Liu, Z.; Zhang, X.; Chan, S.H.; Wang, Y. Dynamic performance of a high-temperature PEM (proton exchange membrane) fuel cell—Modelling and fuzzy control of purging process. *Energy* **2016**, *95*, 425–432. [[CrossRef](#)]
64. Oh, K.; Jeong, G.; Cho, E.; Kim, W.; Ju, H. A CO poisoning model for high-temperature proton exchange membrane fuel cells comprising phosphoric acid-doped polybenzimidazole membranes. *Int. J. Hydrog. Energy* **2014**, *39*, 21915–21926. [[CrossRef](#)]
65. Jiao, K.; Li, X. Water transport in polymer electrolyte membrane fuel cells. *Prog. Energy Combust. Sci.* **2011**, *37*, 221–291. [[CrossRef](#)]
66. Zhang, J.; Xie, Z.; Zhang, J.; Tang, Y.; Song, C.; Navessin, T.; Shi, Z.; Song, D.; Wang, H.; Wilkinson, D.P.; et al. High temperature PEM fuel cells. *J. Power Sources* **2006**, *160*, 872–891. [[CrossRef](#)]
67. Marandi, S.; Sarabchi, N.; Yari, M. Exergy and exergoeconomic comparison between multiple novel combined systems based on proton exchange membrane fuel cells integrated with organic Rankine cycles, and hydrogen boil-off gas subsystem. *Energy Convers. Manag.* **2021**, *244*, 114532. [[CrossRef](#)]
68. Gholamian, E.; Zare, V. A comparative thermodynamic investigation with environmental analysis of SOFC waste heat to power conversion employing Kalina and Organic Rankine Cycles. *Energy Convers. Manag.* **2016**, *117*, 150–161. [[CrossRef](#)]
69. Meng, T.; Cui, D.; Ji, Y.; Cheng, M.; Tu, B.; Lan, Z. Optimization and efficiency analysis of methanol SOFC-PEMFC hybrid system. *Int. J. Hydrog. Energy* **2022**, *47*, 27690–27702. [[CrossRef](#)]
70. Yoon-Ho, L. Thermo-economic analysis of a novel regasification system with liquefied-natural-gas cold-energy. *Int. J. Refrig.* **2019**, *101*, 218–229. [[CrossRef](#)]
71. Song, J.; Gu, C.-W. Performance analysis of a dual-loop organic Rankine cycle (ORC) system with wet steam expansion for engine waste heat recovery. *Appl. Energy* **2015**, *156*, 280–289. [[CrossRef](#)]
72. Razmi, A.R.; Janbaz, M. Exergoeconomic assessment with reliability consideration of a green cogeneration system based on compressed air energy storage (CAES). *Energy Convers. Manag.* **2019**, *204*, 112320. [[CrossRef](#)]
73. Alliance Consulting International. *Methanol Safe Handling Manual*; Alliance Consulting International: San Diego, CA, USA, 2008; Volume 5, pp. 1–37.
74. Sousa, T.; Mamlouk, M.; Scott, K. An isothermal model of a laboratory intermediate temperature fuel cell using PBI doped phosphoric acid membranes. *Chem. Eng. Sci.* **2010**, *65*, 2513–2530. [[CrossRef](#)]
75. ANSI/ASHRAE Standard 34-2019; Designation and Safety Classification of Refrigerants. ASHRAE: Atlanta, GA, USA, 2019; Volume 2019, pp. 1–52.
76. Ryu, B.R.; Anh, D.P.; Lee, Y.H.; Kang, H.K. Study on LNG cold energy recovery using combined refrigeration and ORC system: LNG-fueled refrigerated cargo carriers. *J. Korean Soc. Mar. Eng.* **2021**, *45*, 70–78. [[CrossRef](#)]